

WATER LEVEL FLUCTUATIONS OF NAMCO LAKE IN TIBETAN PLATEAU OBSERVED FROM RADAR AND LASER ALTIMETRY

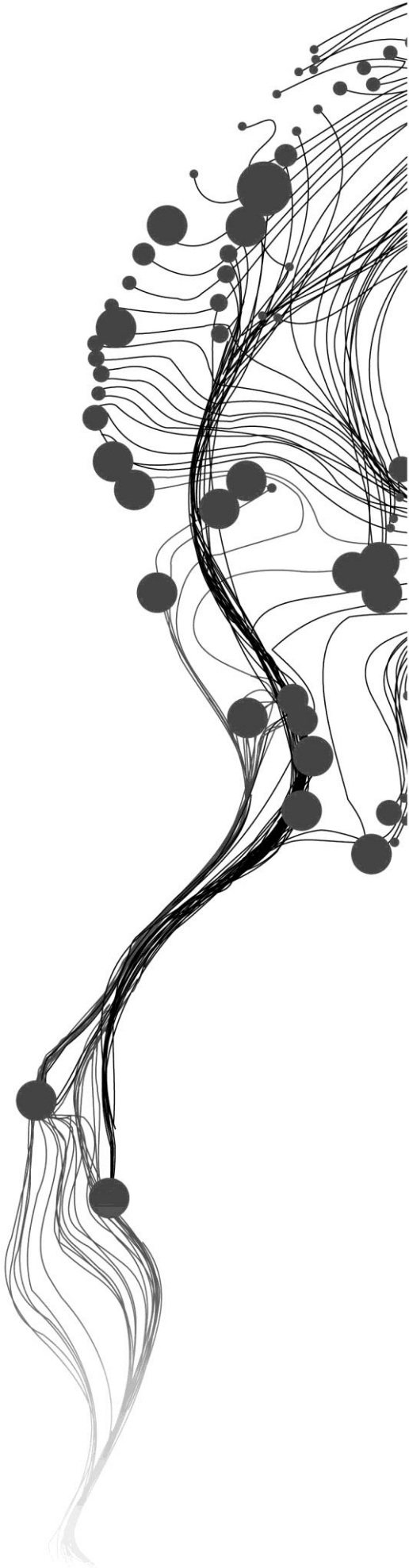
PUKAR MAN AMATYA

February, 2011

SUPERVISORS:

Dr. Ir. Rogier van der Velde

Prof. Dr. Ir. Bob Su



WATER LEVEL FLUCTUATIONS OF NAMCO LAKE IN TIBETAN PLATEAU OBSERVED FROM RADAR AND LASER ALTIMETRY

PUKAR MAN AMATYA

Enschede, The Netherlands, February, 2011

Thesis submitted to the Faculty of Geo-Information Science and Earth Observation of the University of Twente in partial fulfilment of the requirements for the degree of Master of Science in Geo-information Science and Earth Observation.

Specialization: Water Resource and Environmental Management

SUPERVISORS:

Dr. Ir. Rogier van der Velde

Prof. Dr. Ir. Bob Su

THESIS ASSESSMENT BOARD:

Prof. Dr. Ing. Wouter Verhof (Chair)

Prof. Dr. Ir. Nick van de Giesen (External Examiner, Delft University of Technology)

DISCLAIMER

This document describes work undertaken as part of a programme of study at the Faculty of Geo-Information Science and Earth Observation of the University of Twente. All views and opinions expressed therein remain the sole responsibility of the author, and do not necessarily represent those of the Faculty.

ABSTRACT

This study investigates the response of the Namco Lake water budget to changing atmospheric forcings over the period 2003 to 2009. The Namco Lake is a lake with a closed water balance situated on the Tibetan Plateau at an elevation of more than 4700 meter above sea level. This region of Tibetan Plateau has been largely free from anthropogenic influences. As such, any fluctuations in area and level can be associated to the changes in sink (evaporation) and sources (precipitation and runoff) of the lake imposed by atmospheric forcings.

In this thesis, the lake area is derived from ASAR wide swath mode images and water level from space borne radar (ENVISAT RA-2) and laser (ICESat) altimeters. It is shown that in the period from 2003 to 2009 the lake area has grown by 17 km² (0.86 %) and, as a result, a water level rise of more than 2.0 m is observed by the altimeters. The validation of the satellite observed lake level against in-situ measurements from 2007 up to 2009 demonstrates an excellent agreement with a Root Mean Squared Difference (RSMD) of less than 0.15 m.

Precipitation, evaporation and runoff from the catchment area are considered to be factors contributing to the lake growth. These variables were, however, not measured at Namco Lake over the period from 2003 to 2009. Further investigation on the cause of the lake increase relied, therefore, on nearby measurements and readily available products. The rainfall data provided by the Global Land Data Assimilation System (GLDAS) show annually precipitation did not change much. Moreover, evaporation measurements over the nearby Tibetan Selin Co and Yamdrok Yamtso Lake show decreasing trends. This suggests that the runoff into the lake must be increasing.

Part runoff increase is a result from the melting of frozen soil water, with other major contribution from glacier melt water. Increase in runoff is because of air temperature rise on the catchment as the result of less snowfall over the years decreasing the albedo of the region. Rise in temperature was observed for both warm and cold seasons. This rise of temperature for both seasons helps prolong the ablation period. Rainfall in this high region falls in the form of snow during cold season. Seasonal GLDAS rainfall analysis reveals decrease in rainfall in cold season, supporting the rise of temperature during the cold season. Rainfall during warm season increased from 2006. High rainfall decreases the albedo of the region by melting snow from surface wetting which in turn facilitates glacier melt.

Keywords: Tibetan Plateau, Namco Lake, SAR, ENVISAT RA-2, ICESat, Lake area, Lake level.

ACKNOWLEDGEMENTS

First and foremost I would like to thank my first supervisor Dr. Rogier van der Velde for his support and encouragement which motivated me to carry out this thesis. He always had his door open for me, whenever I had some problems. I appreciate the way he forced me to solve the problems myself. Countless hours spent reviewing my thesis and comments helped me improve my writing and thesis as a whole.

I would also like to thank my second supervisor Prof. Dr. Bob Su for reviewing my thesis and comments. My sincere gratitude for facilitating dialogues between us and ITP-CAS for providing in-situ water level data for validation.

Dr. Suhayb Salama's help during my proposal writing period for ordering data is very much appreciated.

My sincere thanks to ESA, NSIDC and ITP-CAS for providing free data, without which my thesis would not have been possible.

I would like to thank my entire family member and friends for their love and support throughout 18 months. Nepalese community past and present for maintain family environment and for all the fun parties and trips across Europe.

WREM 2009 batch mates are acknowledged for all the fun and worst times shared together.

Finally, I would like to thank NUFFIC, ITC, Water Resource faculty and city of Enschede for providing me with this unique opportunity to experience Dutch culture and attain higher education.

TABLE OF CONTENTS

1.	Introduction.....	1
1.1.	Background.....	1
1.2.	Research Problem.....	2
1.3.	Research Objectives.....	2
1.4.	Research Questions.....	2
2.	Study Area and Data.....	3
2.1.	Study Area.....	3
2.2.	In-situ Data.....	5
2.2.1.	Water level.....	5
2.2.2.	Ground meteorological station.....	6
2.3.	SAR data.....	6
2.4.	Altimetry.....	7
2.4.1.	ENVISAT Radar Altimeter (RA-2).....	9
2.4.2.	Ice Cloud and Land Elevation Satellite (ICESat).....	10
2.5.	CMORPH: precipitation data sets.....	11
2.6.	GLDAS land surface simulations.....	12
3.	Methods.....	13
3.1.	Lake area extraction.....	13
3.1.1.	Filtering.....	14
3.1.2.	Image co-registration.....	14
3.1.3.	Terrain Correction.....	14
3.1.4.	Import image and extract area of interest.....	15
3.1.5.	Image Stack.....	15
3.1.6.	Segmentation.....	15
3.2.	Altimetry.....	16
3.2.1.	ENVISAT RA-2.....	16
3.2.2.	ICESAT.....	18
3.2.3.	Validation.....	18
3.1.	CMORPH and GLDAS data processing.....	19
4.	Results and Discussion.....	21
4.1.	Lake Area Extraction.....	21
4.2.	Water Level.....	26
4.3.	Precipitation.....	29
4.4.	Evaporation.....	31
4.5.	Runoff.....	33
5.	Conclusions and Recommendations.....	37
5.1.	Conclusions.....	37
5.2.	Recommendations.....	37
	List of References.....	39
	Appendices.....	42

LIST OF FIGURES

Figure 1. Location of Namco Lake on Tibetan Plateau	3
Figure 2. Namco catchment with location of stations.....	4
Figure 3. In-situ water level measurement reference level.....	5
Figure 4. In-situ water level anomalies (2007 – 2008)	5
Figure 5. Principle of altimetry	8
Figure 6. GLAS instrument making measurement from ICESat while orbiting the Earth by Deborah McLean.....	10
Figure 7. Flowchart of lake area extraction	13
Figure 8. ENVISAT ground track	16
Figure 9. Plot of water level for 4 GDR points within the lake.....	17
Figure 10. ICESat ground track	18
Figure 11. Namco catchment and GRID cell distribution	19
Figure 12. Filtering result of a ERS SAR image acquired on 1992-06-18. (A) Original SAR image acquired on 1992-06-18. (B) Image after applying 3×3 Gamma Map filter. (C) Image after applying 5×5 Gamma Map filter. (D) Image after applying 7×7 Gamma Map filter.	22
Figure 13. (A) 7×7 filtered image acquired on 1992-06-18. (B) 7×7 filtered image acquired on 1992-08-27. (C) Mean image resulted from stacking two images A and B respectively.....	23
Figure 14. Typical ERS SAR image with lake coverage. (A) SAR image on 1992-06-18. (B) SAR image on 1992-07-04.	23
Figure 15. Filtering result of ASAR image. (A) Original ASAR WSM image acquired on 2003-08-02. (B) Image after applying 3×3 Gamma Map filter. (C) Image after applying 5×5 Gamma Map filter. (D) Image after applying 7×7 Gamma Map filter.	24
Figure 16. Histogram of filtered image	25
Figure 17. Image segmentation	25
Figure 18. Lake Area variations for month of August 2003-2009.....	26
Figure 19. ENVISAT water level 2002 – 2009.....	26
Figure 20. ICESat water level 2002 – 2009	27
Figure 21. In-situ – Altimeter correlation for ENVISAT and ICESat.	28
Figure 22. ENVISAT and ICESat water level difference	28
Figure 23. Monthly CMORPH and Bangoin station precipitation.....	30
Figure 24. Monthly GLDAS and Bangoin station precipitation.....	30
Figure 25. (A) CMORPH – Station correlation. (B) GLDAS – Station correlation.....	31
Figure 26. Annual sum of GLDAS rainfall on Namco catchment.	31
Figure 27. Annual sum of land evaporation from Namco catchment.....	32
Figure 28. Location of Selin Co and Yamdrok Yamsto Lake	33
Figure 29. Annual sum of GLDAS snowfall and corresponding mean air temperature	34
Figure 30. Seasonal variation of mean air temperature and GLDAS rainfall in cold season (left) and warm season (right) during 2003 – 2009.....	35

LIST OF TABLES

Table 1: Specification of ERS and ENVISAT.....	6
Table 2: Specifications of ASAR IM and WSM.....	6
Table 3: Three different range resolution mode of RA-2.....	9
Table 4: List of ICESat campaigns.....	11
Table 5: Specification of available CMORPH data.....	12
Table 6: Atmospheric forcing datasets.....	12
Table 7: Water level for October, 2007 from ICESat, ENVISAT and in-situ.....	27
Table 8: Ellipsoid and Geoid used by ENVISAT and ICESat respectively.....	28
Table 9: Comparison of geoid height given in ENVISAT RA-2 and ICESat data sets for December 6, 2008.....	29

ABBREVIATIONS

a.s.l	Above sea level
AFWA	Air Force Weather Agency
AGRMET	Agricultural Meteorology modelling system
AMSU-B	Advanced Microwave Sounding Unit
ASAR	Advanced Synthetic Aperture Radar
CMAP	Climate Prediction Center Merged Analysis Precipitation
CMORPH	Climate Prediction Center Morphing method
CPC	Climate Prediction Center
DORIS	Doppler Orbitography and Radio-positioning Integrated by Satellite
ENL	Equivalent Number of Look
ENVISAT	Environmental Satellite
ERS	European Remote Sensing Satellite
ESA	European Space Agency
GDAS	Global Data Assimilation System
GDR	Geophysical Data Records
GES DISC	Goddard Earth Science Data and Information Services Center
GLA14	Global Land Surface Altimetry Data
GLAS	Geoscience Laser Altimetry System
GLDAS	Global Land Data Assimilation System
HDISC	Hydrological Data and Information Service Center
ICESat	Ice Sea and Land Elevation Satellite
IM	Image Mode
IR	Infrared
IRI	Institute for Climate and Society
ITP-CAS	Institute of Tibetan Plateau Research, Chinese Academy of Sciences
LIS	Land Information System
LRR	Laser Retro-Reflector
MWR	Microwave Radiometer
Nam-MI	Namco Monitoring and Research Station for Multisphere Interactions
NASA	National Aeronautics and Space Administration
NCDC	National Climatic Data Center
NCEP	National Centers for Environmental Prediction
NOAA	National Oceanic and Atmospheric Administration
NSIDC	National Snow and Ice Data Center
PMW	Passive Microwave
RA-2	Radar Altimeter-2
SAR	Synthetic Aperture Radar
SSM/I	Special Sensor Microwave Imager
TMI	TRMM microwave Imager
WMO	World Meteorological Organisation
WSM	Wide Swath Mode

1. INTRODUCTION

1.1. Background

Tibetan Plateau is known as the roof of the world and is located in Central Asia at an elevation of about 4000 m. Beniston & Rebetez (1996), Liu et al. (2009b) have shown that climate change has a more pronounced effect on high elevated areas. As such, global warming is expected to have a significant impact on the Tibetan Plateau (Liu & Zhang, 1998). Liu & Chen (2000) investigated the air temperature from 97 stations on the Tibetan Plateau and found that most of the Tibetan Plateau have experienced significant warming of about 0.16°C/decade since mid 1950s. This warming rate exceeds the trends observed at others part of the northern hemisphere and the same latitude zones, especially during winters. Precipitation has increasing trend in eastern and central part, while western part has decreasing trend (Xu et al., 2008). Change of the climate on Tibetan Plateau not only has profound effect on local weather, but also affects the atmospheric circulation over entire northern hemisphere (Zheng & Li, 1999; Zhou et al., 2009).

The Tibetan Plateau is known as the water tower of Asia. Several rivers, such as Brahmaputra, Ganges, Indus, Yangtze and Yellow river, flow from the Plateau to various regions in Asia supporting hundreds of millions of people downstream. It is, therefore, of great importance to quantify available water resources on the Plateau; especially in today's changing climate scenario. There are more than 1500 lakes on the plateau ranging in size from 0.01 km² to 4000 km². Inland lakes, in general, are sensitive to changes in climate variables such as air temperature, precipitation, evaporation and permafrost degradation (Bianduo et al., 2009). Water balances of high elevation inland lakes on the Tibetan Plateau are closed and have largely been free of anthropogenic influences. Hence, the water balance of high elevation lakes that have been free from anthropogenic influences is representative for climate regime of Tibetan plateau.

Various studies have been carried out in past to monitor lake growth (Liu et al., 2010; Liu et al., 2009a; Reis & Yilmaz, 2008; Wald, 1990) using remote sensing observations acquired from the visible part of the spectrum. However the visible part of the spectrum is affected by the atmosphere and cannot penetrate cloud, which often restricts the availability of useful observations. The use of microwave remote sensing observation can overcome these limitations. Active microwave measurements obtained via the Synthetic Aperture Radar (SAR) technique provide not only day/night coverage, but also accommodates high spatial resolution needed to detect subtle changes in the lake dimensions. The backscatter from the smooth water surface is typically lower than that of the surrounding land because specular scattering mechanism prevails. Based on these properties, microwave images are an excellent tool in environmental monitoring application such as lake area monitoring (Telmer & Costa, 2007), flood monitoring (Oberstadler et al., 1997) or coastline extraction (Beniston & Rebetez, 1996).

Water level fluctuations are driven by water inputs/outputs (Birkett, 1995; Mercier et al., 2002). Inputs are primarily precipitation, surface runoff and groundwater, whereas outputs are evaporation, groundwater seepage and outflow from the lake. As such monitoring water level of lakes with closed water balance is useful to study the regional effect of climate change. Owing to the harsh climatic condition and remoteness of the plateau it is not always possible to monitor the water levels on ground. Monitoring elevation from space via altimetry is often the only practical means for remote areas such as Tibetan Plateau. Although most altimeters were primarily designed for ocean application, its ability to monitor

water level of inland lakes has been highlighted by Crétaux & Birkett (2006), Frappart et al. (2006), Medina et al. (2008), Mercier et al. (2002).

1.2. Research Problem

Recent studies (Liu et al., 2010; Liu et al., 2009a; Zhu et al., 2010) have shown that on the Tibetan Plateau lakes are increasing in size due to climate change. These studies are based upon few images acquired in the visible part of the electromagnetic spectrum over 10 year periods because cloud coverage restricted the data collection of the earth surface.

Cloud coverage does not affect microwave observations. Synthetic Aperture Radar (SAR) images can, therefore, be utilized to monitor lake extents at a higher temporal resolution than would be possible with optical/thermal remote sensing. On the other hand the size of lake area can be also associated with water level in the lake, which can be observed from space using altimeters onboard the Environmental Satellite (ENVISAT) and ICESat. As such, both lake extents observed by SAR and water levels measured via altimetry can provide supporting evidence for lake growth noted at very low temporal resolution in previous studies.

1.3. Research Objectives

The main objective of this research is to evaluate the response of Tibetan Namco Lake under a changing climatic condition.

The Specific objectives of this research are to:

1. Check the suitability of different types of SAR images (e.g. ERS SAR, ASAR image mode/wide swath) for the extraction of the extent of the Namco Lake.
2. Derive water level from space borne radar and laser altimetry products and compare the results with in-situ data.
3. Determine annual precipitation for the catchment using remote sensed product (CMORPH) and land surface model (GLDAS).
4. Investigate the actual cause of variation in lake area and water level.

1.4. Research Questions

1. Is the trend of water level in accordance with the surface area of the lake?
2. How consistent is the water level derived from space borne altimeters as compared to the in-situ data?
3. What are the causes of increase/decrease of lake dimensions?

2. STUDY AREA AND DATA

2.1. Study Area

Namco lake (30°30'–30°55' N, 90°16'–91°3' E) is the second largest lake on the Tibetan Plateau with an area of about 1920 km² and is located at an elevation of 4718 m above sea level (a.s.l) (Figure 1). This is a closed lake with drainage area of 10776 km² as shown in Figure 2. Precipitation is the main source of water over the lake surface and in the catchment area which enters the lake as runoff. In the south of the catchment lies Nyainqentanglha mountain range with peaks well above 6000 m (a.s.l) which is covered with over 100 glaciers. The melt from the northern glaciers flows directly into the lake and contribute to water level. Land use in Namco drainage area consists for the past centuries of occasional pilgrimage. As such, water levels of the lake are not affected by any anthropogenic factors. This makes Namco an ideal candidate for studying the climate change.

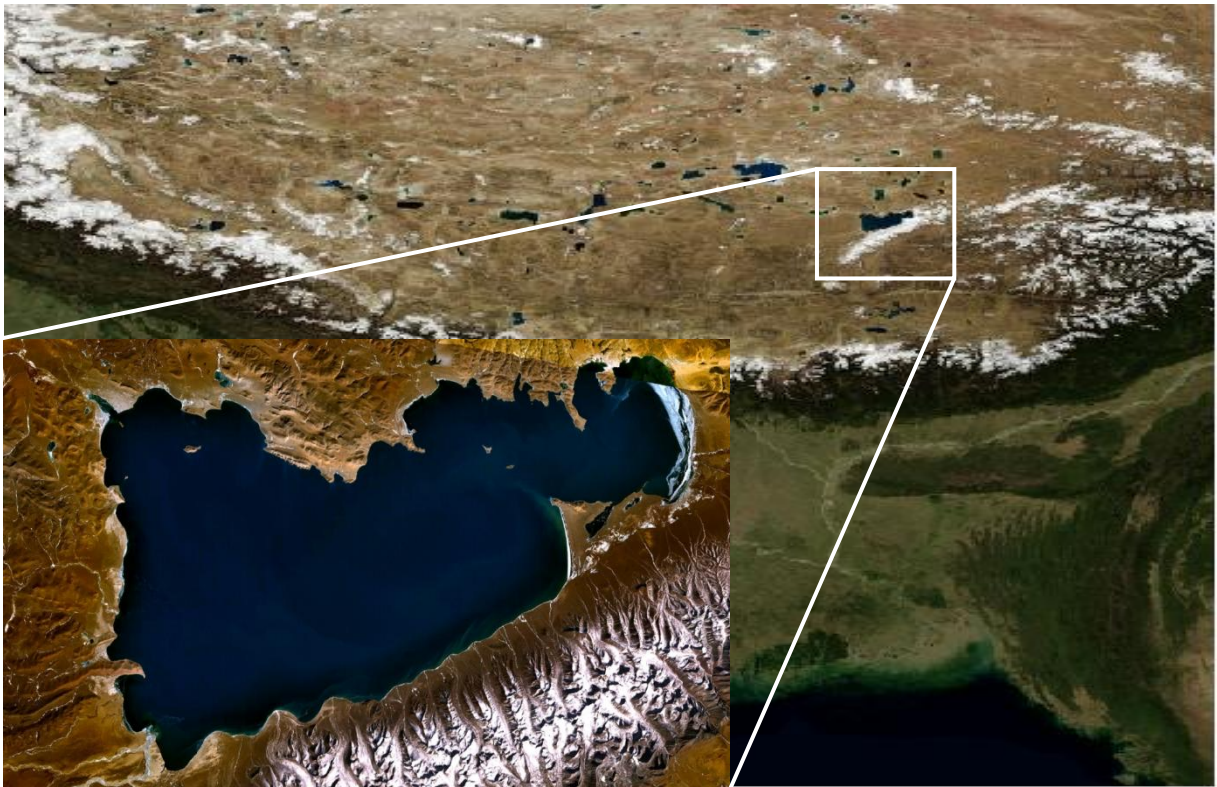


Figure 1. Location of Namco Lake on Tibetan Plateau

At the southeastern shore of the Namco Lake, the Institute of Tibetan Plateau Research, Chinese Academy of Sciences (ITP-CAS) established the Namco Monitoring and Research Station for Multisphere Interactions (Nam-MI) (N30°46.44', E90°59.31', 4730 m) in 2005 (Figure 2). The main purpose of this station is to collect hydrological data and conduct studies on atmospheric physics, lake-climate interaction, glacier melt, chemical properties of water and vegetation change. Before 2005 the Namco catchment was not equipped with a meteorological station. Therefore, previous studies (Liu et al., 2010; Zhu et al., 2010) on the lake relied on meteorological variables measured at nearby stations.

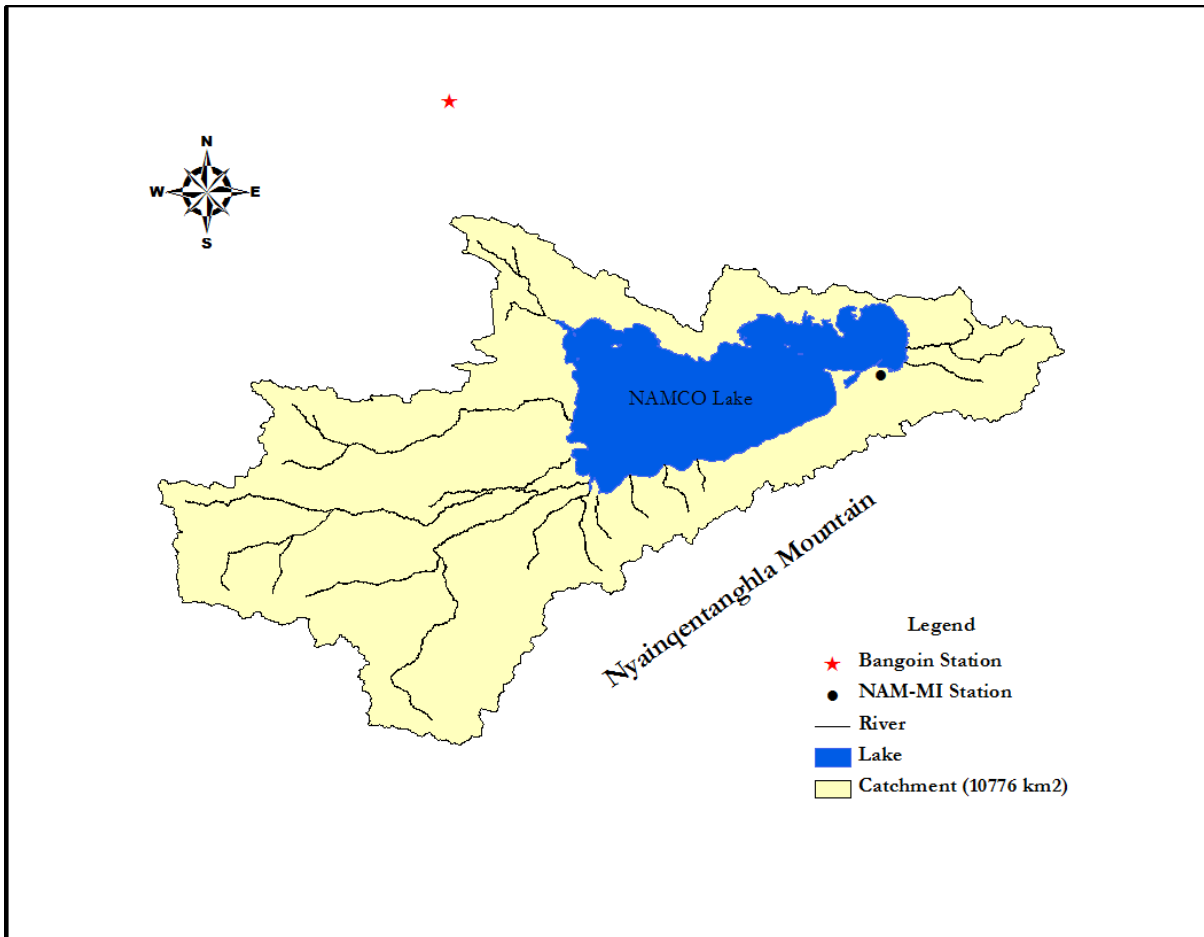


Figure 2. Namco catchment with location of stations

The nearest meteorological station is Baingoin ($31^{\circ}23' N$, $90^{\circ}01' E$). Based on data collected at this station, the mean annual temperature in this region is $-1.1^{\circ}C$ with lowest temperature of $-11^{\circ}C$ in January. On average the total annual amount of rainfall is about 310 mm. As the region is affected by the Asian Monsoon, rain occurs primarily in the summer with its peak intensity in the months of July, August and September. Winters are typically dry and cold with temperatures below freezing from October to April. The little amount of winter precipitation falls in the form of snow, which melts along with the frozen soil water in spring.

2.2. In-situ Data

2.2.1. Water level

Namco Lake in-situ water level data was provided by ITP-CAS. This water level data is measured at Nam-MI station (Figure 2). The in-situ data are relative to a reference level and measured manually as shown in Figure 3.



Figure 3. In-situ water level measurement reference level

Figure 4 shows the time series of water level anomalies. Due to harsh climatic condition on the plateau during the winter season, daily water level measurements are only available for the months of May to December from 2007 onwards. Measured water levels follow a seasonal trend with highest fluctuations observed for the month of July – August (monsoon period) each year. Even in this short period a steadily increasing trend is observed in the water level, which could be the results of changing atmospheric forcings.

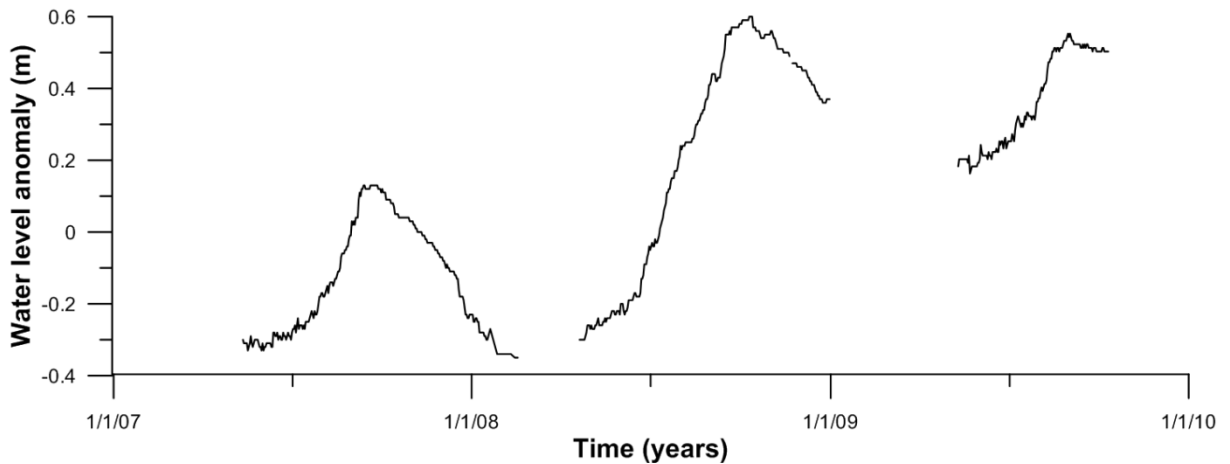


Figure 4. In-situ water level anomalies (2007 – 2008)

2.2.2. Ground meteorological station

Daily temperature and precipitation measurements are available from Bangoin station (31°23' N, 90°01' E, see Figure 2). Next to Nam-MI station, this is the station closest to the Namco Lake and holds a data record from 1954 up to now. The data is obtained from National Climatic Data Center (NCDC, <http://www.ncdc.noaa.gov/oa/ncdc.html>), which is supported by the World Meteorological Organisation (WMO). The data sets in this database are subjected to an extensive quality control. As such, the meteorological variables measured at Bangoin station are considered to be reliable.

2.3. SAR data

In this thesis, an attempt has been made to monitor the lake area using Synthetic Aperture Radar (SAR) data sets collected by instruments onboard satellites of European Space Agency (ESA). Since 1991 the ESA launched three satellites with SAR instrumentation: the ERS (European Remote sensing Satellite) -1, ERS-2 and ENVISAT (Environmental Satellite). Both ERS SAR sensors are single channel systems that can operate in a single mode at a fixed image swath. The ENVISAT SAR includes several modes and the angle of antenna beam can be programmed to one of the seven positions. General specifications of both products are given in Table 1.

Table 1: Specification of ERS and ENVISAT

Sensor	Satellite	Launch date	Band	Polarization	Spatial resolution	Incidence Angle
SAR	ERS-1 & -2	1991, 1995	C	VV	25m	23°
ASAR	ENVISAT	2002	C	Dual-pol	25m, 150m &1000m	15° - 45°

For this thesis, level 1 geocoded (GEC) ERS-1/-2 and ENVISAT data sets acquired in two modes have been used. The text below gives details on the SAR images provided from the ERS-1/-2 and ENVISAT platforms.

European Remote Sensing satellite (ERS-1) with the first Synthetic Aperture Radar (SAR) system onboard was launched on July 1991. ERS-2 was launched on April 1995, positioned one day behind ERS 1 on the same track. ERS-1 ended its mission in 2000 whereas ERS-2 is still operational. For this research SAR image mode with a 25 m spatial resolution is used. SAR image mode has swath width of 100 km and revisit time of 35 days. Quota of 155 ERS SAR images was provided free of charge by ESA. We ordered 22 ERS-1, 40 ERS-2 from ESA archives which covered the lake. A list with the dates of the acquisitions is provided in APPENDIX A.

Table 2: Specifications of ASAR IM and WSM

Type	Spatial resolution	Swath width	Revisit time
Image mode (IM)	25 m	100 km	35 days
Wide swath mode (WSM)	150 m	405 km	3 days

The Advanced SAR (ASAR) instrument onboard the Environmental Satellite (ENVISAT) launched on March 2002 extends the SAR mission flown on the ERS. ASAR uses an active phased-array antenna as apposed to a short physical antenna used by ERS SAR, with incidence angles between 15 and 45 degrees (ESA, 2007). With ASAR it is possible to obtain images of the same area from several orbits at different view angles. This improves the potential revisit time to a daily coverage near the poles and up to a weekly coverage at the equator. For this research ASAR image mode and wide swath mode (WSM) were acquired (Table 2). ASAR image mode has the same specification as of ERS SAR image mode. The WSM includes a larger swath width (400 km) which opens up new possibilities for applications that require a more frequent

revisit. In total, 224 ENVISAT ASAR images were provided free of charge by ESA. We ordered 94 IM and 7 WSM from the archives. A list with the dates of the acquisitions is provided in APPENDIX B.

2.4. Altimetry

Altimetry measures the time required for a pulse, released nadir to the target to reach the earth surface and return back. The measured time multiplied by the speed of light gives the two way distance between the target surface and the satellite i.e. two way range. Signals when travelling through the atmosphere gets decelerated by water vapour and ionization. Once the influences by these phenomena are corrected for, the final range is estimated.

$$\text{Two way range} = c \times t \quad (1)$$

Where, c is the velocity of light and t is the two way travel time. The range is calculated as follows:

$$\text{The range to the target} = \frac{c \times t}{2} \quad (2)$$

The altitude of satellite is the distance of the satellite from reference surface (ellipsoid). Therefore, precise orbit determination is important for maintaining the accuracy of altimeter products and is done by satellite tracking. The measurement techniques are:

- Doppler Orbitography and Radio-positioning Integrated by Satellite (DORIS) which makes accurate measurement of Doppler shift of radio frequencies transmitted from ground beacons to satellite. The receiver onboard the satellite analyses the frequency to calculate its velocity relative to the earth. This velocity is then fed into orbit determination model to determine the position of satellite in orbit.
- Global Positioning system (GPS) on board the satellite can be used for precise and continuous tracking of the satellite.
- Laser tacking system consists of a reflector on board the satellite which acts as a target for ground satellite ranging stations.

The surface height is then calculated by subtracting the corrected range from the altitude of the satellite from the reference surface (Figure 5).

$$\text{Height} = \text{Altitude of the satellite} - \text{Corrected range.}$$

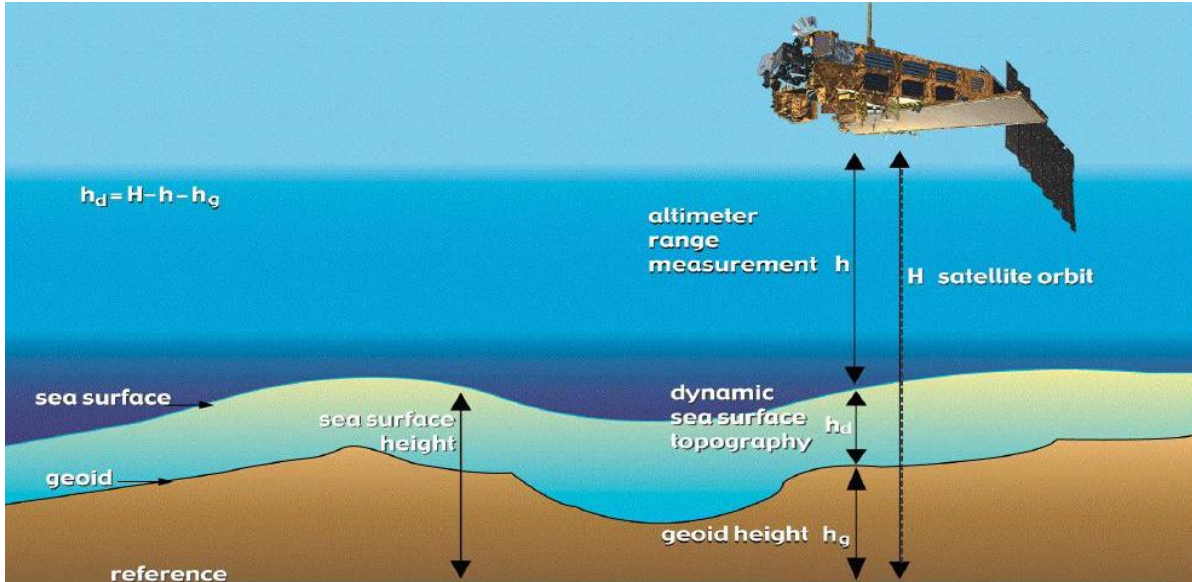


Figure 5. Principle of altimetry

Range corrections are calculated by satellite based instruments or by models. These corrections are available within the level 2 altimetry data set and have to be subtracted from the range. Necessary range corrections are described below:

- **Ionosphere Correction**

This correction is applied to take account of path delay of radar signal due to electrons present in the atmosphere. Ionosphere is the uppermost part of the atmosphere ranging between 60 and 80 km, with its highest concentration between 250 and 400 km above the land surface. For ENVISAT it is calculated by combining measurement at two different frequencies (Ku band and S band) or by DORIS measurements. This correction is not needed for ICESat as laser is not affected by ionosphere.

- **Dry troposphere correction**

This correction is applied to take account of path delay of return signal due to atmospheric dry gas refraction. This correction is calculated by using metrological models considering surface temperature and pressure.

- **Wet troposphere correction**

This correction is applied to take account of path delay of signal due to liquid in the atmosphere. This correction is calculated by using microwave radiometers but for areas such as land and coastal area by meteorological models.

- **Earth tide**

This correction takes account of solid earth variation due to the attraction of sun and moon. It is calculated by models.

- **Pole tide**

This correction takes account of ocean response to variation of both solid earth and ocean due to centrifugal potential generated by small perturbation to earth's rotation axis. It is also calculated by using models.

For this research two different space borne altimeter products are used, which are:

- ENVISAT Radar Altimeter 2 (Radar)
- Ice Sea and Land Elevation Satellite (Laser)

Radar altimeter uses microwaves and can penetrate cloud whereas laser uses wavelength in visible ranges thus becoming useless when clouds are present. Advantage of laser over radar lies in its narrow footprint width 70 m diameter (ICESat) compared to 19 km footprint of ENVISAT RA-2. Retrieved elevation is average of all the topography within a footprint, so small footprint is more desired.

2.4.1. ENVISAT Radar Altimeter (RA-2)

RA-2 altimeter was launched onboard ENVISAT on March 2002 as a follow on altimetry mission to ERS-1 and ERS-2 by European Space Agency. The objectives of RA-2 are to provide enhancements to ERS ocean and ice mission, improve the quality of measurement as well as improve the monitoring capacities for complex terrains such as land, lakes, wetlands, rivers etc.

The Radar altimetry mission onboard ENVISAT comprises of 4 instruments:

- RA-2: a multi-resolution, self-adaptive, dual frequency radar altimeter
- MWR: a dual-frequency nadir-viewing microwave radiometer
- DORIS: a dual-frequency Doppler tracking system for orbit estimation
- LRR: a laser retro-reflector for tracking.

The RA-2 sensor provides measurements of the elevation by transmitting radar pulses at nadir in two frequencies: 13.575 GHz (Ku-band) and 3.2 GHz (S-band). One of the major improvements over ERS altimeters is the addition of second band (3.2 GHz, S-band) which allows compensation for delay due to ionospheric electron density (Benveniste et al., 2001). The distance between the satellite and reflecting body (ocean, land and ice) is determined by precisely measuring the travel time of radar pulse from the satellite to the surface and back. The altitude of the satellite above the reference ellipsoid is computed using a precise orbit determination system DORIS. Then the surface height is determined by subtracting the corrected range from satellite altitude.

RA-2 has three range resolution (Table 3) adapted to different sensing scenario (ocean, sea ice, ice sheet and land). This is another advantage over the ERS altimeters which suffered with data loss over difficult terrain. RA-2 automatically changes the resolution according to the surface type in order to keep the echoes within the tracking window, thus avoiding losing track.

Table 3: Three different range resolution mode of RA-2

Bandwidth (MHz)	Resolution (m)	Range window (m)
0.5	0.5	64
80	2	256
20	8	1024

The RA-2 provides 18 range measurements per second which corresponds to along track sampling distance of about 400m. The mission has temporal resolution of 35 days. Lake Namco is over flown by RA-2 descending orbit number 262. For this research we use ENVISAT RA-2 1 Hz range measurement contained in Geophysical Data Records (GDR) (ESA, 2009) from cycle 10 to cycle 92 (October 2002 to November 2009). The range value provided in GDR product is the average of 20 range measurements

covering about 8 km along track segment. GDR's are available after 30 days from the acquisition date and are processed offline in a ground station to obtain better estimates. The data set was obtained via European Space Agency.

2.4.2. Ice Cloud and Land Elevation Satellite (ICESat)

Ice Cloud and land elevation satellite (ICESat) was launched on January 12, 2003 by NASA. The primary objective of ICESat is to quantify ice sheet mass balance and understand how changes in the Earth's atmosphere and climate affect the polar ice masses and global sea level (NASA, 2002). ICESat will also measure global distributions of clouds and aerosols for studies of their effects on atmospheric processes and global change, as well as land topography, sea ice, and vegetation cover.

Geoscience Laser Altimeter System (GLAS) on ICESat quantifies the distance from satellite to earth's surface by measuring the two-way travel time of an electromagnetic pulse in the visible part of spectrum to the reflecting object. GLAS transmits laser energy at both 1064 nm (for surface) and 532 nm (for atmosphere). This allows co-located elevation and atmospheric data to be obtained simultaneously. GLAS uses integral star tracker and gyros for determining laser orientation and Global positioning system (GPS) to keep track of its own location. The GLAS sends laser pulses at a rate of 40 per second, with each a footprint of 70m separated by about 170 m in the along track direction as shown in Figure 6.

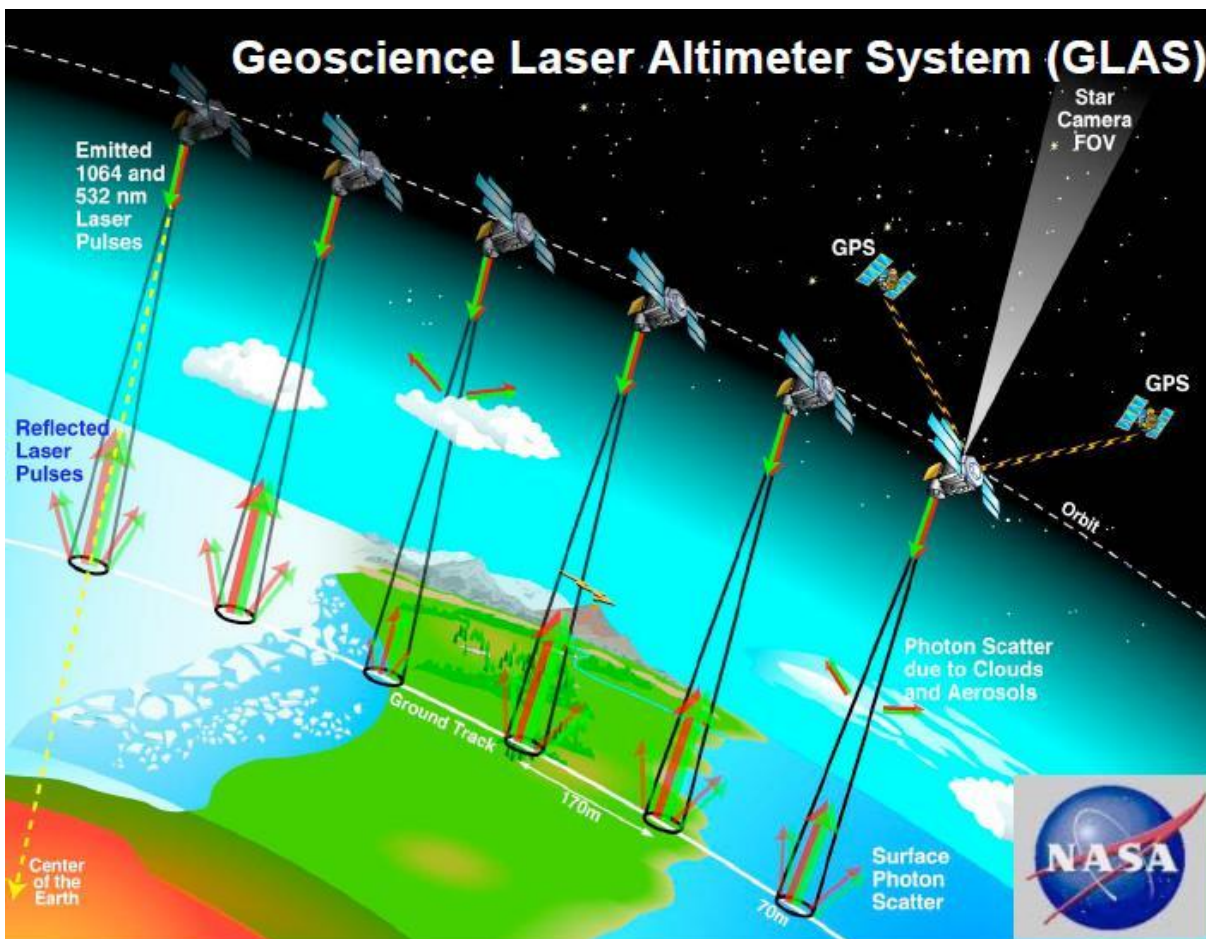


Figure 6. GLAS instrument making measurement from ICESat while orbiting the Earth by Deborah McLean

GLAS has three lasers, but only one laser is operational at a given time to ensure the continuity of the mission as one laser was expected to have a life of 1-1.5 years. Laser 1 was operational from February 20, 2003 to March 29, 2003. After the failure of laser 1, operating plan was modified to 30 days operation period, three times per year and repeat time was changed to 91 days. Laser 3 failed in 19 October, 2008. Laser 2 failed on 11 October, 2009 ending the campaign. Complete list of ICESat campaigns are given in Table 4.

Table 4: List of ICESat campaigns

Campaign period	Start date	End date	Operating time (days)	Orbit days
Laser 1	20-Feb-03	29-Mar-03	38	8
Laser 2a	25-Sep-03	19-Nov-03	10/47	8/91
Laser 2b	17-Feb-04	21-Mar-04	34	91
Laser 2c	18-May-04	21-Jun-04	35	91
Laser 3a	3-Oct-04	8-Nov-04	3	91
Laser 3b	17-Feb-05	24-Mar-05	36	91
Laser 3c	20-May-05	23-Jun-05	35	91
Laser 3d	21-Oct-05	24-Nov-05	35	91
Laser 3e	22-Feb-06	28-Mar-06	35	91
Laser 3f	24-May-06	26-Jun-06	35	91
Laser 3g	25-Oct-06	27-Nov-06	34	91
Laser 3h	12-Mar-07	14-Apr-07	34	91
Laser 3i	2-Oct-07	5-Nov-07	35	91
Laser 3j	17-Feb-08	21-Mar-08	34	91
Laser 3k	4-Oct-08	19-Oct-08	16	91
Laser 2d	25-Nov-08	17-Dec-08	23	91
Laser 2e	9-Mar-09	11-Apr-09	34	91
Laser 2f	30-Sep-09	11-Oct-09	12	91

For this research Global land surface altimetry data (GLA14) (Zwally et al., 2003) from 2003 – 2009 was used. The data set was provided by National Snow and Ice Data Center (NSIDC). ICESat precision is about 2 cm in flat surfaces with elevation accuracy of ± 15 cm (Shuman et al., 2006).

2.5. CMORPH: precipitation data sets

Infrared (IR) data are available globally and can be extracted through the geostationary satellites. IR measures the cloud top brightness temperature and associates it with rainfall. However, these temperatures do not correlate very well with rainfall, sometimes with no rainfall directly below the coldest cloud. Passive microwave (PMW) sensors have dual frequencies, lower frequency senses the thermal emissions from raindrop and higher frequency senses the scattering of upwelling radiation from the earth surface by ice particles in the rain layer. PMW are sensitive to moisture in the cloud and are considered more accurate than IR. Its temporal sampling is low compared to IR sensors due to its low orbit.

Numbers of techniques are developed to combine the data from these two sensors to take the advantage of each. One technique is making use of low orbital PMW exclusively, and transferring its features via spatial propagation information obtained from geostationary IR satellite during the period when PMW data are not available (Joyce et al., 2004). This technique is called Climate Prediction Center Morphing method i.e. CMORPH.

CMORPH uses half hourly brightness temperature from geostationary satellites. For PMW precipitation it uses estimates from National Oceanic and Atmospheric Administration (NOAA) polar orbiting meteorological satellites. The PMW instruments used aboard these satellites are Advanced Microwave Sounding Unit (AMSU-B), Special Sensor Microwave Imager (SSM/I) and TRMM microwave Imager (TMI).

CMORPH data is available via NOAA, Climate Prediction Center (CPC) (http://www.cpc.noaa.gov/products/janowiak/cmorph_description.html). Specification of available data set is given in Table 5.

Table 5: Specification of available CMORPH data

Temporal Resolution	Spatial resolution	Time Period
3 hours	25 km	December 2002 - present
Daily	25 km	February 2005 - present
30 minutes	8 km	2002

For this thesis, 3 hourly data aggregated to daily (2003-2009) available via The International Research Institute for Climate and Society (IRI), Columbia University, USA was used. This data set is available via OPENDAP server and can be downloaded directly for MATLAB processing from:

http://iridl.ldeo.columbia.edu/SOURCES/.NOAA/.NCEP/.CPC/.CMORPH/.daily_calculated/.mean/.morphed/.cmorph/.

2.6. GLDAS land surface simulations

Global Land Data Assimilation System (GLDAS) drives land simulation models in an uncoupled mode from the atmosphere, forced with a combination of remote sensing and simulated atmospheric data within the Land Information System (LIS) (Kumar et al., 2006). For NOAA model, GLDAS product is available at a 3 hourly or monthly temporal resolution with 0.25° spatial resolution from 2000 up to now. The land model is driven by atmospheric forcings (Table 6) supplemented by parameter data (vegetation, LAI, soil, elevation).

These products can be downloaded from Hydrological Data and Information Service Center (HDISC), a component of NASA Goddard Earth Science Data and Information Services Center (GES DISC). The data are available in GRIB or NETCDF format. For this thesis NOAA 0.25° rainfall, evaporation and snowfall data were used.

Table 6: Atmospheric forcing datasets

Dataset	Description	Date
GDAS	The Global Data Assimilation System (GDAS) is the global operational weather forecast model of NCEP	2000 - present
AGRMET shortwave flux	LDAS estimates global, downward shortwave, and longwave radiation fluxes using a procedure from the Air Force Weather Agency's (AFWA) Agricultural Meteorology modelling system (AGRMET).	2001 - present
AGRMET longwave flux		
CMAP Precipitation	The Climate Prediction Center Merged Analysis Precipitation is a technique which produces pentad and monthly analyses of global precipitation.	2001 - present

3. METHODS

3.1. Lake area extraction

The grey tone of a SAR image represents the strength of backscattering from terrain because specific objects on the earth surface scatter radiation differently. Water surfaces, in the absence of strong wind and chlorophyll act as a smooth surface, for which specular reflection prevails. As a result water surfaces produce a low backscatter response and appear as dark in the image. Land appears brighter than water because of the vegetation and surface height variations cause land surfaces to appear rough. These qualities of SAR images can be utilized to classify land and water based on thresholding. Before the thresholding technique can be applied, several pre-processing steps should be under taken. A schematization of the ordering of these steps is shown in Figure 7, which is briefly described in the text below.

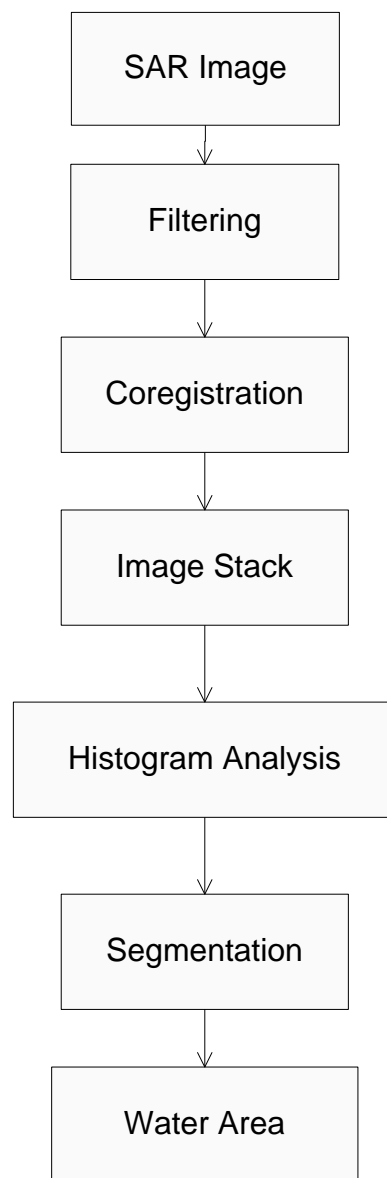


Figure 7. Flowchart of lake area extraction

3.1.1. Filtering

Speckle is granular noise that exists in every SAR image and degrades the quality of image. Speckle is the result of coherent sensing technique employed by radar and is caused by mixing of signal from multiple distributed targets. Multi look processing is used to reduce the speckle in which several look at the target is taken in a signal swipe and are averaged to reduce the noise.

The image used in this thesis is multi looked but still contained noise, so moving window filtering technique was applied. Our main goal is to separate land and water, so it is necessary that the edges are well preserved. Gamma map filter is selected, which is an adaptive filter specifically developed for reducing the noise in radar images. This filter performs spatial filtering on each individual pixel using grey level values from the surrounding pixels within a selected window size. Special attention should be given to the size of the window because small window will result in less effective noise removal where as large window will not preserve fine details. For this thesis we tested the gamma map filter using 3×3 , 5×5 and 7×7 window.

3.1.2. Image co-registration

ERS SAR and ASAR dataset contained image which were obtained at different dates from different orbit. In order to perform image stacking these images should match exactly. This is done by using co-registration function in NEST, which will co-register one or more slave image to a master image. This process is fully automatic; it does not require manual selection of ground control points for the master and slave image. All the images used in co-registration should be of same projection, if not the slave image must be reprojected into the projection of master image. The image co-registration is accomplished in three steps:

- **Create Stack**

Create stack collocates master and slave image. The slave image is resampled to share the same geopositioning information and image size of the master image.

- **Ground control points selection**

A set of uniformly distributed ground control points in the master image are generated and their corresponding position in the slave image are computed. This process is fully automatic.

- **Wrap**

This function maps the slave pixel into the master pixels and generates the final co-registered image.

3.1.3. Terrain Correction

Image not taken at sensor nadir will have some distortion due to topographic variation within the scene and tilt of the sensor. Terrain correction is intended to remove these distortions and was done using Range Doppler Terrain Correction in NEST. This process was also used to extract image geoinformation for the image to be exported into ENVI for further processing. Range Doppler terrain Correction uses range Doppler orthorectification method for geocoding SAR image. It utilises orbit information from metadata, radar timing annotations, slant to range conversion parameters in combination with SRTM DEM to derive the precise geolocation information.

3.1.4. Import image and extract area of interest

Terrain corrected images were then imported in ENVI and its coordinate system was converted from lat/lon to UTM for calculation of lake area. Area of interest which included the lake was extracted from the whole image using resize data option in ENVI. Special attention should be given while setting upper left and lower right coordinate, that they remain the same for all the images so that it would not create any problem during image stack procedure.

3.1.5. Image Stack

Image stacking is a procedure of combining two or more co-registered images to enhance the features and suppress noise. Same number of rows and columns, same pixel size and same geoinformation is a must for image stacking. Image stacking was done by writing an IDL code. The code gives mean, standard deviation, coefficient of variation, kurtosis and hysteresis of the combined image. At the end by studying the individual type of stack image decision was made to use mean image for segmentation process.

3.1.6. Segmentation

Segmentation is process of partitioning the image into connected region by combining group of neighbouring pixels with similar values i.e. grey level, texture, edges etc. Thresholds for separating land and water are selected by creating a histogram for all the pixels within the study area. The peaks and valley in the SAR image are used then to set the limits. A sharp contrast appears in the grey level of water and land in the SAR image. Water with its low scattering appears as dark tone and land with brighter tones. So, a typical radar image with less noise will produce a bimodal peak with the first peak representing the limits for water and the later for land. A DN value in between the peaks was selected as the limit to separate land and water. Segmentation was done by using segmentation image function in ENVI. Once the segmentation was done it was converted to vector using post classification function in ENVI. The vector was then converted into shape file and the area of the lake was calculated on pixel basis on ArcGIS.

3.2. Altimetry

3.2.1. ENVISAT RA-2

Lake Namco is overflowed by the ENVISAT's RA-2 in a descending orbit, number 262. Geophysical data records contained 4 points which lie within the lake separated 8km apart from each other (Figure 8). Every 1-Hz measurement available in the GDR is the average of 20 18-Hz measurements.

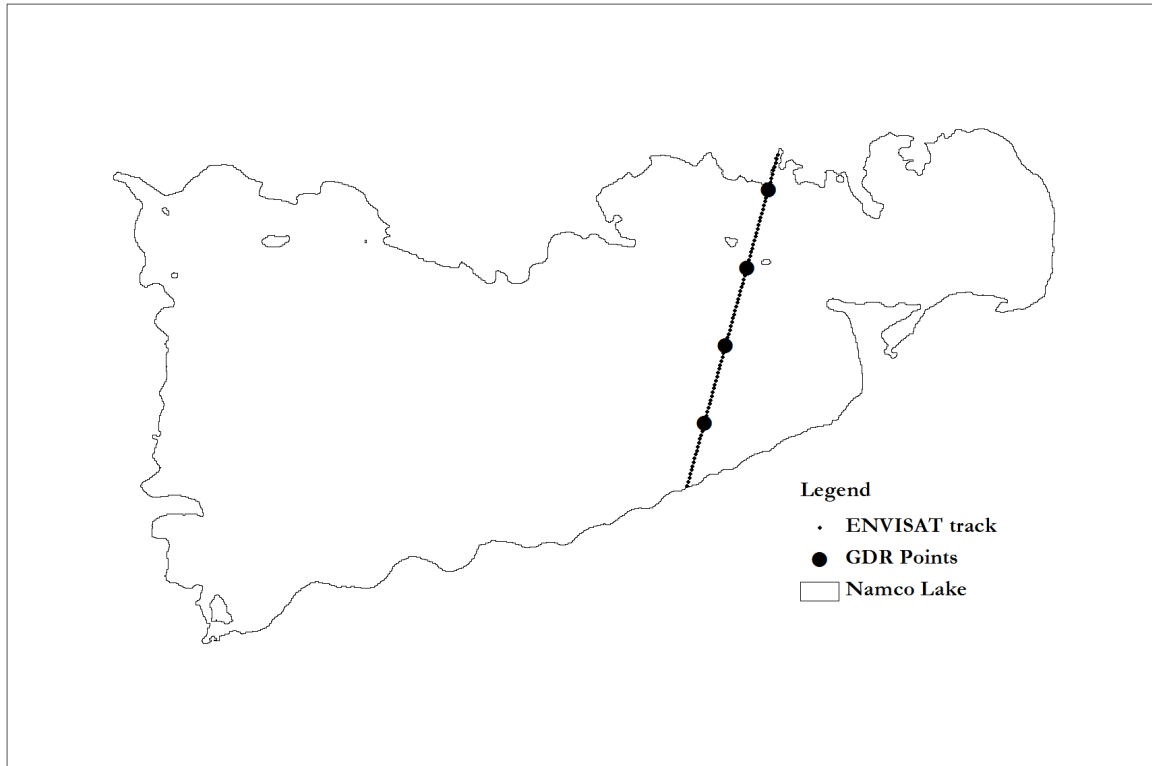


Figure 8. ENVISAT ground track

ENVISAT is primarily designed to monitor ocean surface. Ocean surface is assumed to be homogeneous as a result 20 range measurements are averaged and a single range value separated by 8km apart is provided. It becomes important that we select only those points that are obtained by averaging 20 range measurements. ENVISAT RA-2 has large footprint and also its ground track does not pass through the same exact place, it is designed to vary by ± 1 km. As a result, it is very important to manually see the height obtained near the edges of lake to prevent land heights beings considered.

A plot of 4 points for each month before applying the selection criteria is shown in Figure 9. There are huge differences in elevation between the points especially during rainy season (May – July). Radar signal is affected by snow, rain, the signal gets attenuated as a result of which wrong elevation are calculated (Quarty et al., 1998).

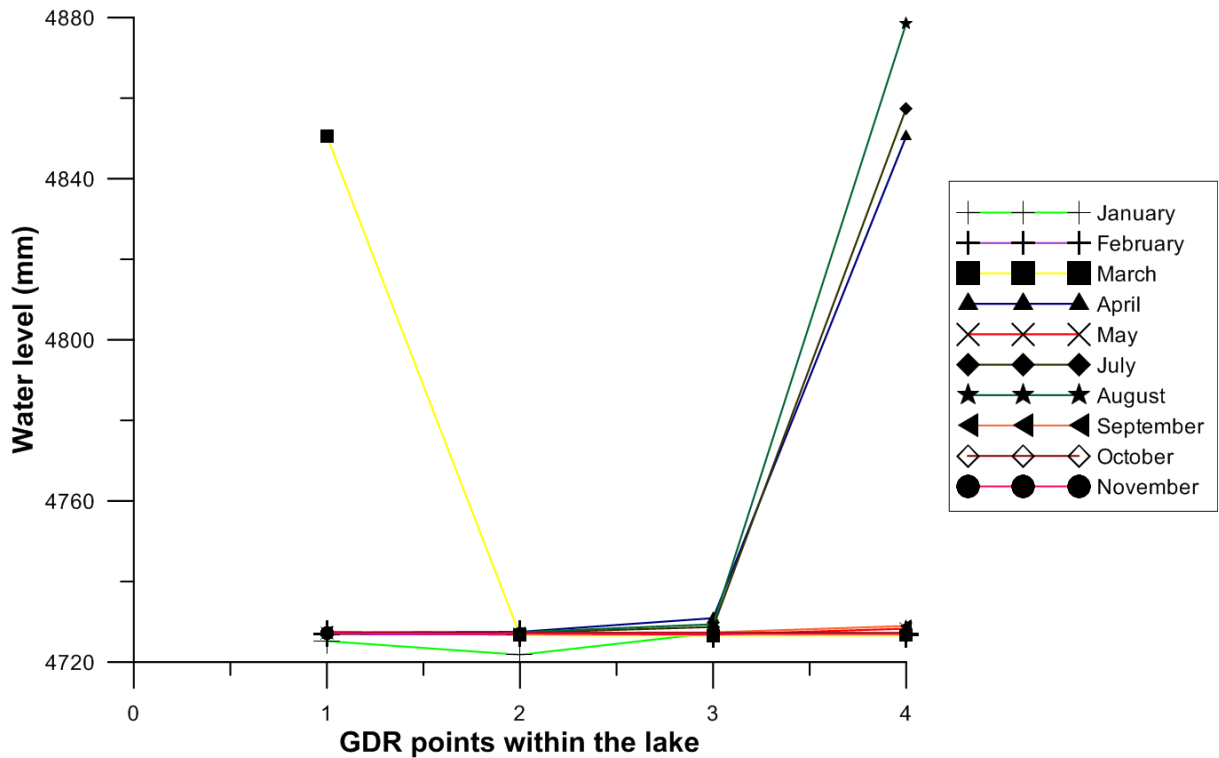


Figure 9. Plot of water level for 4 GDR points within the lake

A special data selection criterion was selected to select number of valid points. These checks were carried out using Basic Radar Altimetry Toolbox (BRAT). The criteria's are:

Number of valid 18 Hz point for 1 Hz measurement = 20

Data Quality flag = 0

Altimeter surface flag type = 1 (ice or closed lake)

An altimeter waveform is a histogram of all the energy backscattered from the surface to the satellite. Land surface waveforms are multi-peaked and noisy due to the presence of several reflectors within the footprint. Accurate range measurements are thus obtained by refined procedure known as altimeter waveform retracking. In order to obtain geophysical parameter i.e. range, four type of retrackers are run for all type of surface (ocean, ice, sea ice etc) on ground. They are:

- i. Ocean retracker (Ocean surface)
- ii. Ice 1 retracker (Continental ice sheet and land)
- iii. Ice 2 retracker (ice sheet)
- iv. Sea ice retracker (Sea ice surface)

Even though these retrackers were not developed for continental water, Frappart et al. (2006) and Medina et al. (2008) investigated these retrackers and found that Ice 1 retracker range can also be used for continental water.

The corrections made to range are modelled dry troposphere, wet troposphere, earth tide, pole tide and DORIS ionosphere. Sea state bias was left out because lakes do not behave as open ocean. The lake level

above a reference ellipsoid was then computed by subtracting the corrected range from the satellite altitude. In order to increase the accuracy of the elevation geoid height was added to the elevation. EGM96 geoid heights are presented in the GDR's. The valid points were then averaged to get lake level for a pass.

3.2.2. ICESAT

Data obtained from NSIDC was visualized to see whether it had passes through the lake with the help of GLAS visualizer. Once the pass was detected then elevation, geoid and correction parameters were extracted using NSIDC GLAS elevation extractor tool. Both these tools are IDL based and were download from NSIDC website (<http://nsidc.org/data/icesat/tools.html>).

Corrections needed for ICESat are wet troposphere, dry troposphere and tide correction. Saturation correction is not generally suggested for GLA 14 data (NSIDC, 2009). Once all these parameters were obtained, the corrected elevation was computed by subtracting the corrections. The levels thus extracted are with respect to a reference datum (TOPEX/Poseidon ellipsoid). Due to inhomogeneous mass distribution of the earth the level can be further corrected by considering the height of geoid above/below the reference ellipsoid. EGM2008 geoid is used by ICESat. Final lake level was thus obtained by adding geoid to the corrected elevation. Elevation from all the points within the lake was then averaged to obtain the lake level (Figure 10).

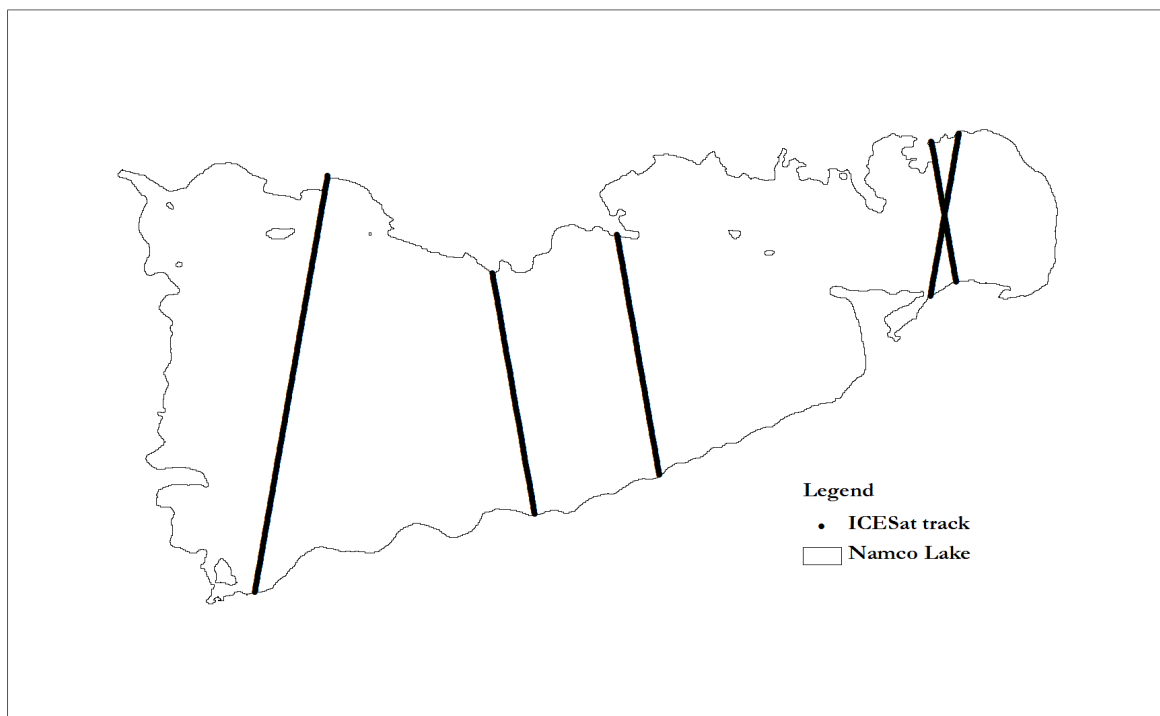


Figure 10. ICESat ground track

3.2.3. Validation

In-situ data provided by ITP was according to a reference level i.e. anomaly, so in order to compare lake level anomaly must be calculated for altimeter data as well. The mean lake level height is calculated by averaging the lake levels for each calculation from 2003 to 2010. The lake level anomaly is then computed by subtracting mean lake level height from individual lake level height. Finally, correlation is computed between two datasets to see how the two datasets correlate to each other.

3.1. CMORPH and GLDAS data processing

Namco catchment was delineated from SRTM DEM using hydro processing tool in ILWIS. $0.25^{\circ} \times 0.25^{\circ}$ grid was created in ArcGIS and was overlaid in the catchment area to determine the number of grid that covered the whole catchment (Figure 11). In total 21 grid units covered the whole catchment. MATLAB code was then prepared for CMORPH and GLDAS data was processed on IDL. Data from the valid grids were then averaged to get monthly rainfall, evaporation and snowfall.

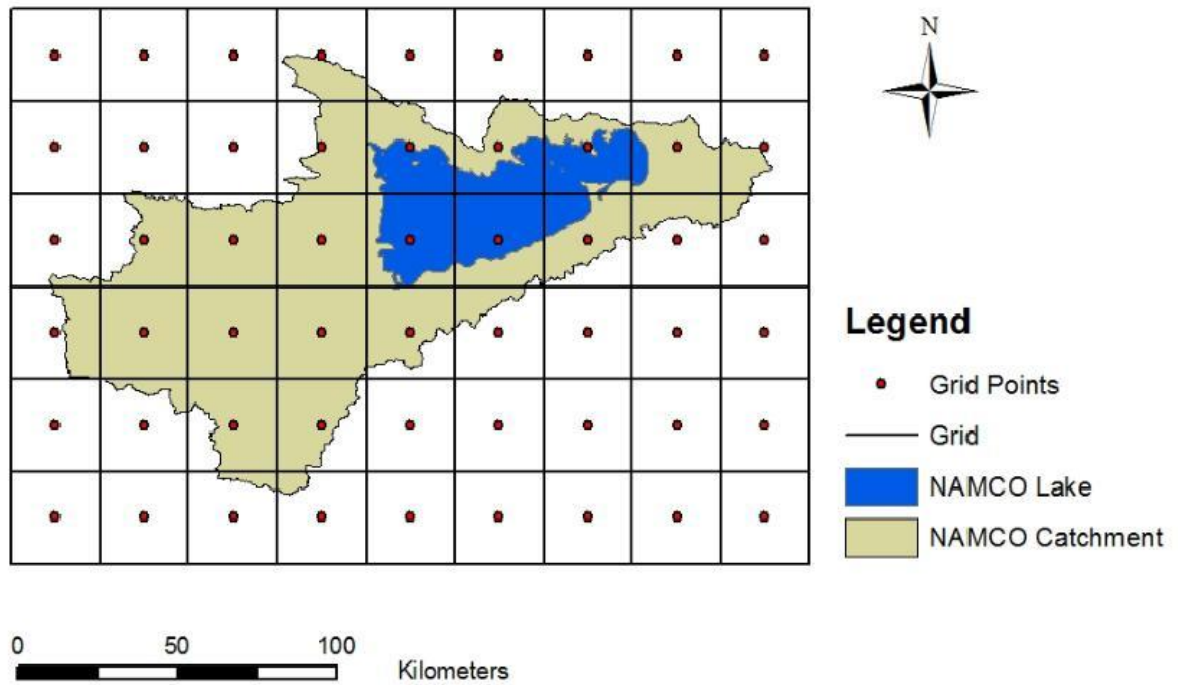


Figure 11. Namco catchment and GRID cell distribution

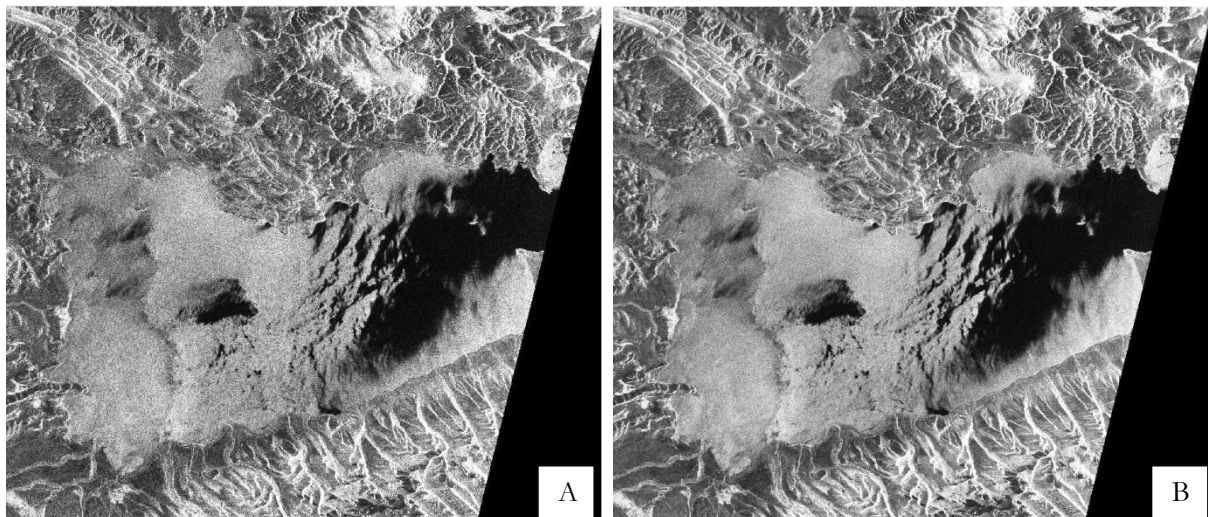
4. RESULTS AND DISCUSSION

4.1. Lake Area Extraction

ERS SAR and ASAR image mode were first filtered to remove speckle. Since not much change was observed temporal image stacking was tested and mean image was generated. This procedure also did not improve the quality image for extracting lake area as a result of which ERS SAR and ASAR image mode was judged unsuitable for extracting area of Namco Lake.

ASAR WSM images had less speckle, so filtering did not bring much change in the image quality. As there were not frequent images available covering Namco Lake in WSM and also clear distinction was observed between land and water, image stacking procedure was not done. Finally, the lake area was calculating using segmentation procedure in ENVI. The results and findings are described in section below.

Figure 12 shows the results of applying different sized moving window filter. Although filtering was able to remove considerable amount of noise, low backscattering property of calm water which makes the water area appear dark was not maintained in the middle portion of the lake. This might be because of high backscattering due to roughness over the water surface which is possibly caused by wind or rain ripples (ESA, 2000). As wind speed and direction data are not available for the time of acquisition of the images, no furthering analysis was performed. Segmenting these images will result in water area being classified as land and manual correcting over this large lake would consume too much time.



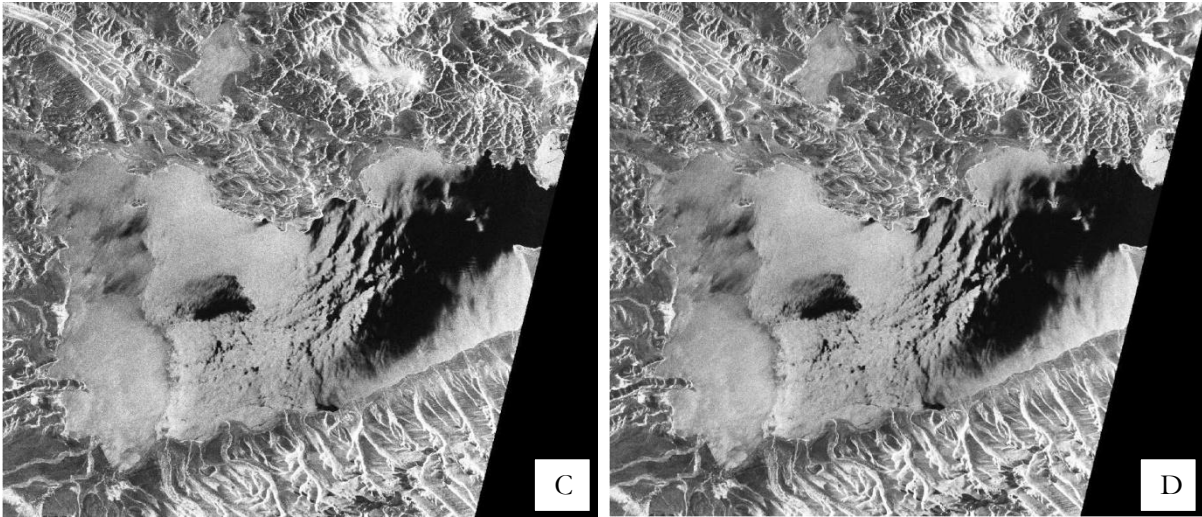
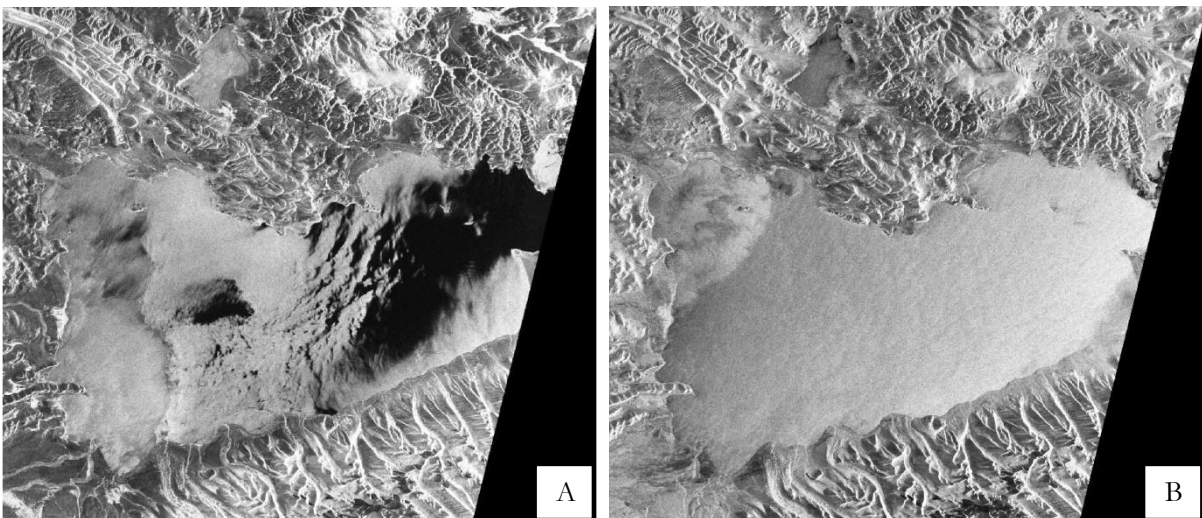


Figure 12. Filtering result of a ERS SAR image acquired on 1992-06-18. (A) Original SAR image acquired on 1992-06-18. (B) Image after applying 3×3 Gamma Map filter. (C) Image after applying 5×5 Gamma Map filter. (D) Image after applying 7×7 Gamma Map filter.

In an attempt to improve the image, the 7x7 filtered images (Figure 12 A and B) were stacked and a mean image was generated (Figure 13 C). The result is an image in which the low backscattering (dark) part of Figure 13 (A) has been replaced by the backscattering in Figure 13 (B) further degrading the darker tone of water.



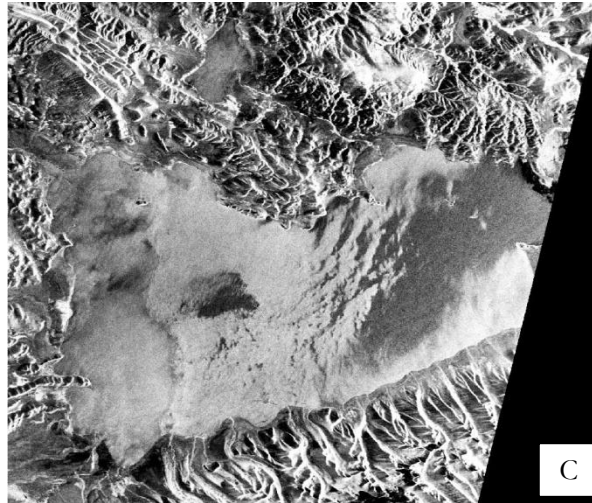


Figure 13. (A) 7×7 filtered image acquired on 1992-06-18. (B) 7×7 filtered image acquired on 1992-08-27. (C) Mean image resulted from stacking two images A and B respectively.

Temporal resolution of SAR and ASAR image is 35 days. Due to the large area of lake and 100 km swath width of the images only half of the lake was covered in an image (Figure 14). Other half was acquired with a time difference of 1 week and sometimes was unavailable. Mosaicing them and image stacking will result in wrong area calculation of the lake which is not desired.

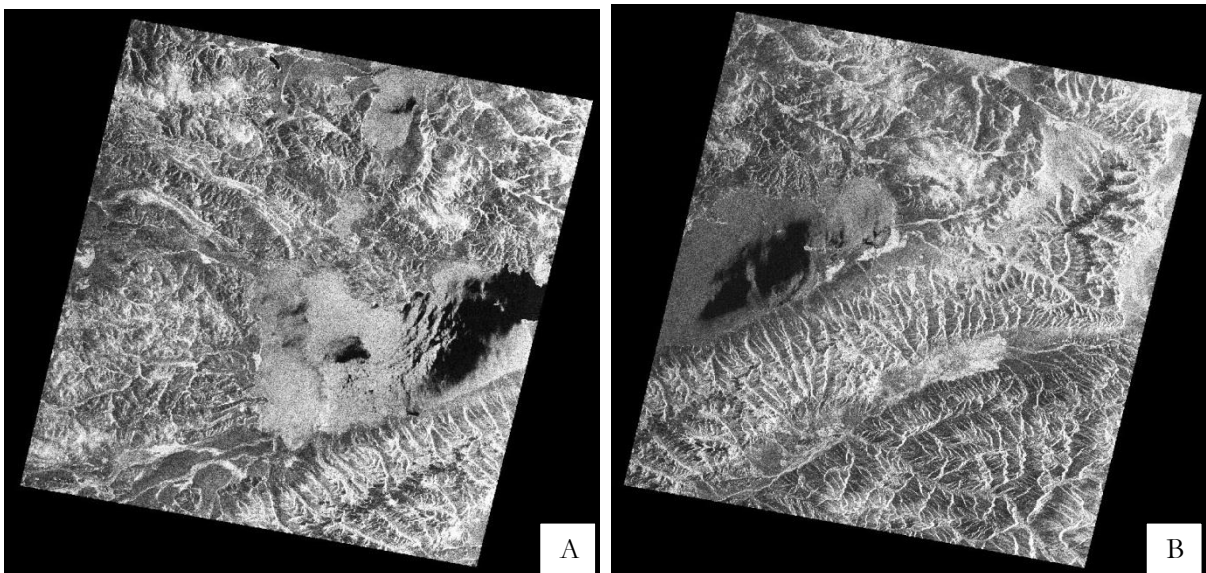


Figure 14. Typical ERS SAR image with lake coverage. (A) SAR image on 1992-06-18. (B) SAR image on 1992-07-04.

ASAR image mode acquisitions have the same specifications and characteristics as ERS SAR data. Results obtained from ASAR are also the same as that of the ERS SAR. So both these products were judged to be not suitable for lake area extraction for this thesis.

Temporal resolution of WSM is 3 days and contains the whole lake in one image. ASAR WSM is multi looked with an equivalent number of looks (ENL) of 12 (Zink et al., 2002) as a result of which contains

less noise than the ERS and ASAR IM. Figure 15 shows subset of ASAR WSM and output images of applying different sized filters. 3×3 window filter (Figure 15 B) was able to remove noise and as we increase the size of the window not much change was observed.

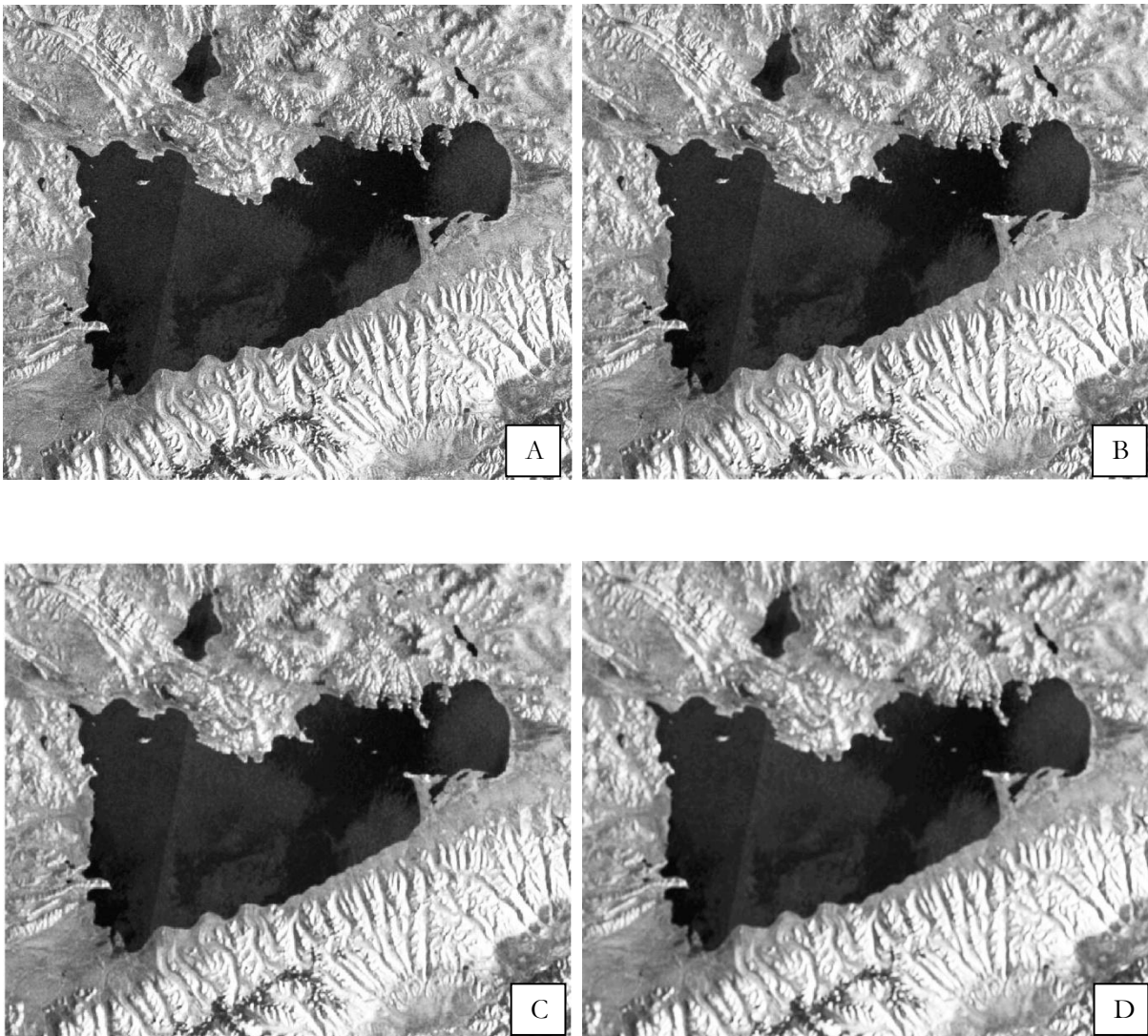


Figure 15. Filtering result of ASAR image. (A) Original ASAR WSM image acquired on 2003-08-02. (B) Image after applying 3×3 Gamma Map filter. (C) Image after applying 5×5 Gamma Map filter. (D) Image after applying 7×7 Gamma Map filter.

Histogram of filtered image gave bimodal peak with front peak representing darker tones while the second representing brighter tones (Figure 16). The value from beginning to the end of the first peak represented the dark region i.e. water. So, for segmentation process maximum and minimum grey scale values from the first peak was chosen to be segmented as water area.

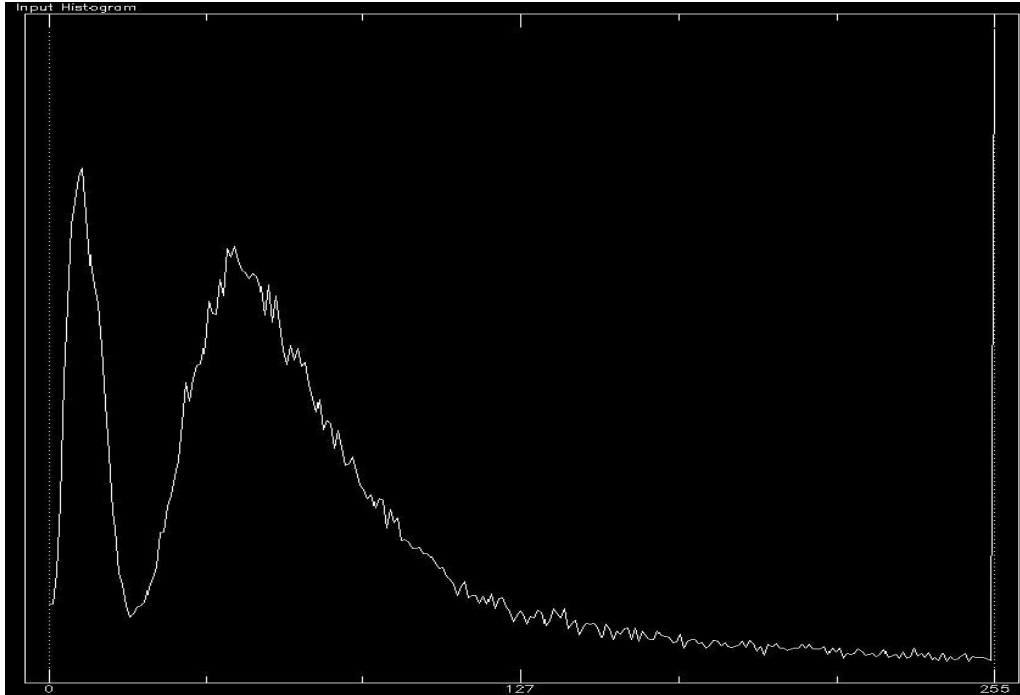


Figure 16. Histogram of filtered image

The result of segmentation is shown in Figure 17. The segmented image was then vectorized and overlaid over the original image to check the extent of lakes calculated. Overclassified regions due to mixed signals mainly near the edges were manually corrected and islands in the middle of the lakes were removed to get the final lake area.



Figure 17. Image segmentation

Due to unavailability of frequent ASAR WSM we used month of August, right after the rainy season when the lake area will be at its maximum to study the change of lake area in response to atmospheric variables. General trend of annual lake area variation is growing (Figure 18), which is in accordance with studies that suggest lakes on Tibetan plateau are growing (Liu et al., 2010; Liu et al., 2009a; Zhu et al., 2010). From 2003 to 2009 the area has increased by 17 km² (0.86 %). The lake area calculated and image dates are given in APPENDIX C.

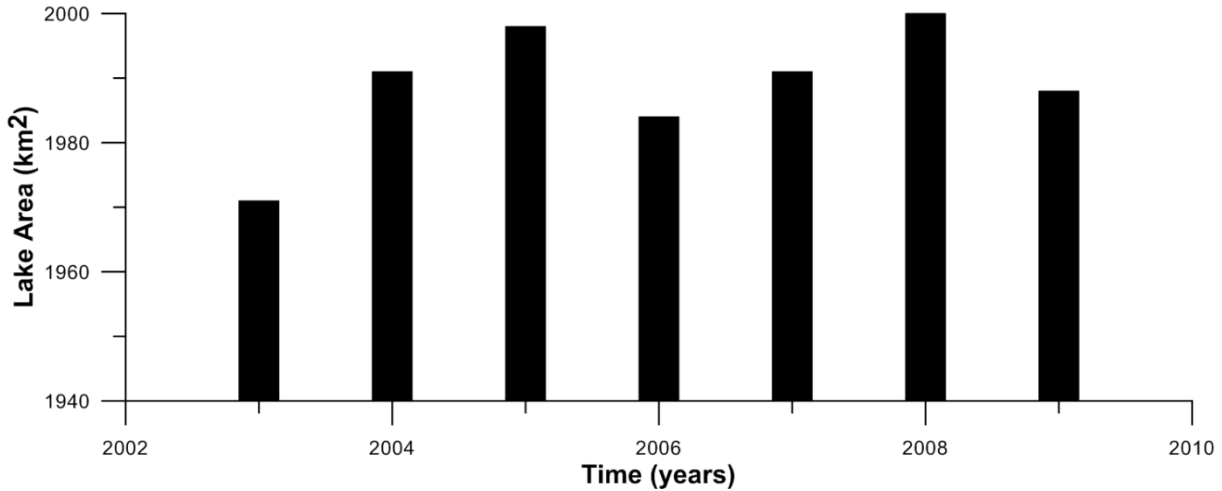


Figure 18. Lake Area variations for month of August 2003-2009.

4.2. Water Level

Water level obtained from ENVISAT RA-2 is shown in Figure 19. Annually water level follows a seasonal trend with lowest water levels recorded in winter seasons and highest during the rainy season. General trend of water level is increasing with highest water level recorded in 2008. Winter water levels for years 2008-2010 is higher than the water levels calculated for entire year of 2003. The water level rose 2.11 m from 4725.163 m of February 1, 2003 to 4727.28 m of October 17, 2009.

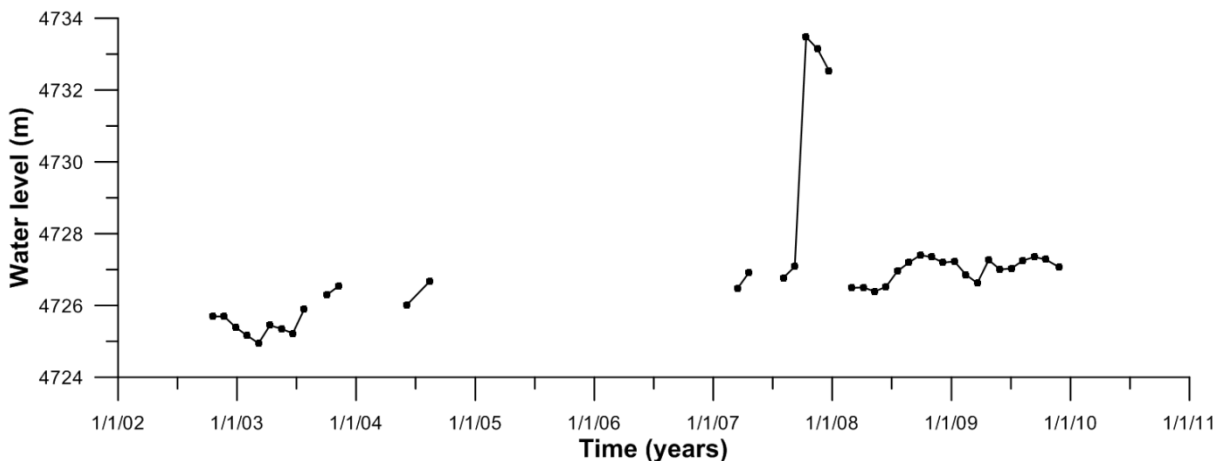


Figure 19. ENVISAT water level 2002 – 2009

In 2007 an abrupt water level rise was found for the month of October, November and December. To check for this abrupt rise we compare this water level with levels from ICESat and in-situ data around the same date (Table 7). Both water levels does not record these high rises. So these ENVISAT values are

considered as outliers and omitted for further analysis. For 2004 - 2007 the data were not available due to sensor calibration while passing through this area. Water Level and measurement dates are given in APPENDIX D.

Table 7: Water level for October, 2007 from ICESat, ENVISAT and in-situ

Method	Date	Water Level (m)
ICESat	10/11/2007	4725.845801
ENVISAT	10/13/2007	4733.478575
In-situ	10/13/2007	0.07

Lake levels calculated by ICESat have a rising trend with largest lake level in October, 2008 (Figure 20). Due to 99 days revisit time of ICESAT, measurements were available only twice a month for the month of March and October. Water level in March is low because it is winter season when there is no rain input as well as water from glaciers as they are frozen. October is just after rainy season with input from rainwater as well as some water from glaciers because temperature must be higher than in March. For 2006 the water levels in March are almost the same as for October of 2004, with water levels in October even higher. The water level rose 2.45 m from 4723.67 m of February 23, 2003 to 4726.12 m of October 9, 2009. Water Level and measurement dates are given in APPENDIX E.

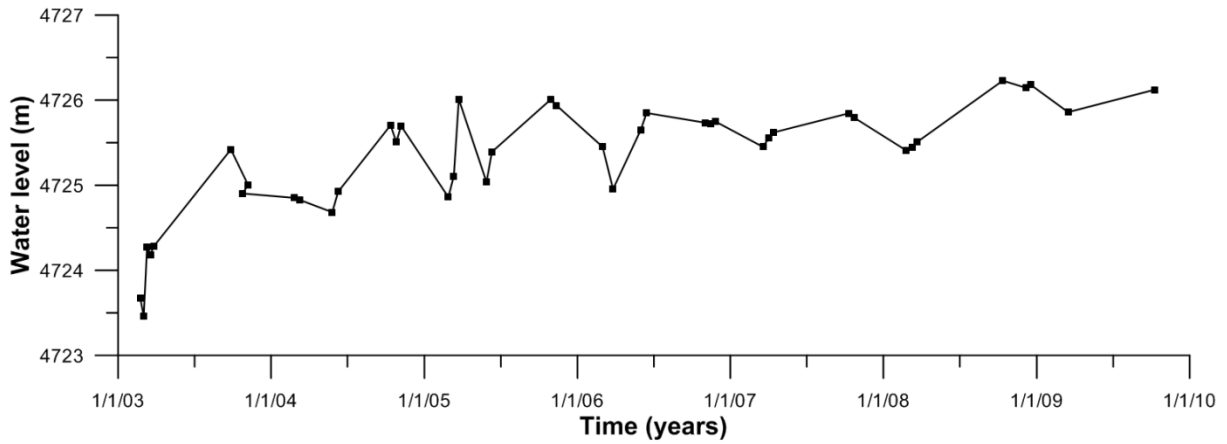


Figure 20. ICESat water level 2002 – 2009

Altimeter lake level data were compared with the in-situ data for time span of 2007-2010. Good fit was found between the altimeters and in-situ water levels. Coefficient of determination (R^2) was found to be 0.86 and 0.95 for ENVISAT and ICESat respectively (Figure 21). The RMSD for ENVISAT is 0.11 m which is the same as found by Frappart et al. (2006). For ICESat the RMSD is 0.14 m. The high RMSD for ICESat can be attributed to the distance of its track from the in-situ measurement site due to its operation pattern change (Figure 10).

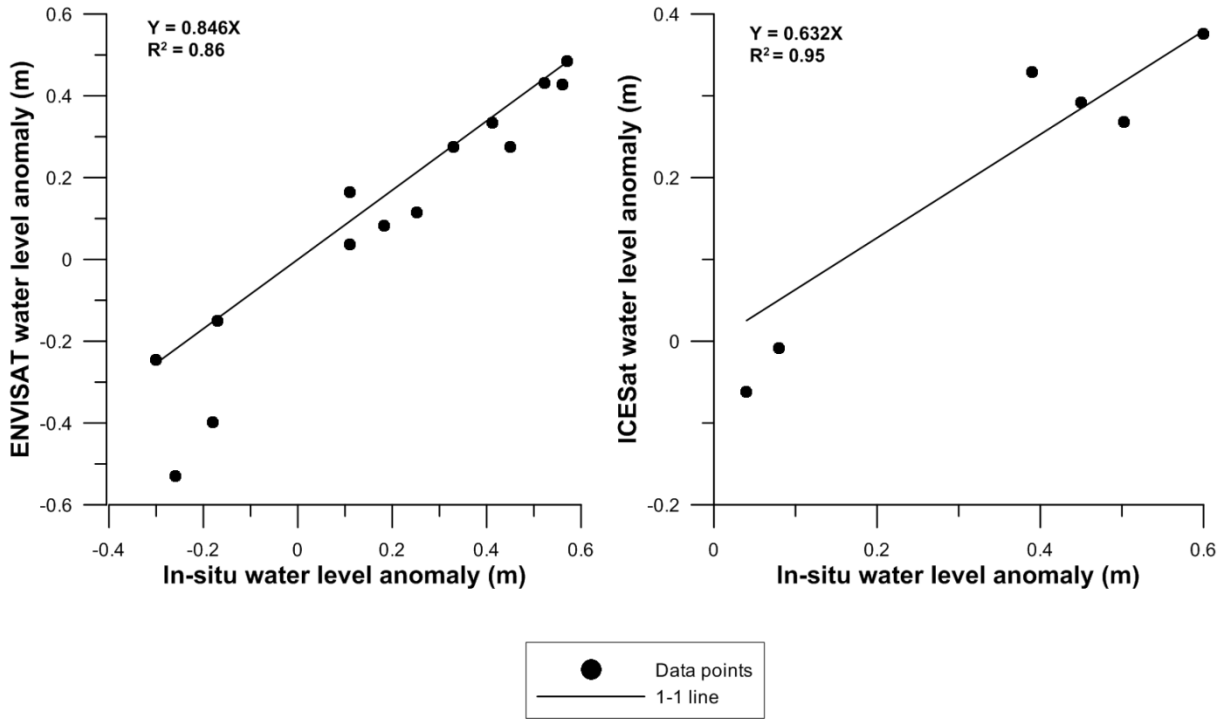


Figure 21. In-situ – Altimeter correlation for ENVISAT and ICESat.

Differences of about 1m are observed in water levels measured by ENVISAT and ICESat (Figure 22). These differences can be explained by difference in reference ellipsoids, geoids (Table 8). On average 0.7 m difference is obtained between WGS-84 and Topex/Poseidon ellipsoids (NSIDC). The range corrections applied on different dates varies according to the track of the satellites affecting the level calculated.

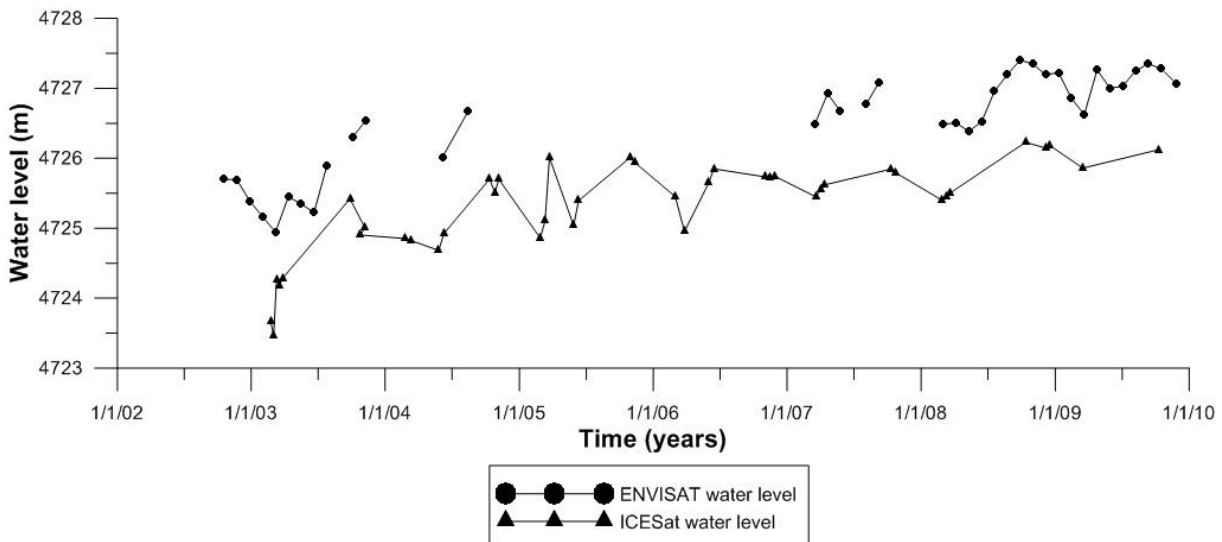


Figure 22. ENVISAT and ICESat water level difference

Table 8: Ellipsoid and Geoid used by ENVISAT and ICESat respectively

Description	ENVISAT	ICESat
Ellipsoid	WGS-84	Topex/Poseidon
Geoid	EGM96	EGM2008

In order to check by how much these two data sets differ, validation must be done at the crossing point of these two tracks. In case of Namco Lake the tracks did not cross within the lake. On December 6, 2008 both altimeters had passes through the lake. Comparison of geoid height provided in the data set revealed EGM96 geoid height used for ENVISAT RA-2 to be 0.95 m lower than the EGM2008 used for ICESat (Table 9). As a result of which lake level obtained from ENVISAT RA-2 was higher than that obtained from ICESat. This suggests that the difference in water level shown in Figure 22 can be reduced by using the same earth gravity models.

Table 9: Comparison of geoid height given in ENVISAT RA-2 and ICESat data sets for December 6, 2008.

Description	ENVISAT	ICESAT	Difference
Mean (geoid)	-35.23 m	-34.28 m	0.95 m
Standard deviation (geoid)	0.14 m	0.01 m	
Number of range points	4	73	
Water level with geoid	4727.19 m	4726.15 m	1.05 m
Water level without geoid	4691.94 m	4691.87 m	0.07 m

4.3. Precipitation

Figure 23 shows a plot of monthly CMORPH catchment and Bangoin station precipitation. In general, during the summer the CMORPH data follows a similar pattern as the measurement at the station but in winter season CMORPH registered considerably high precipitation. Higher precipitation in winter might be attributed to strong scattering by snow/ice surface which may be mistaken for a precipitating cloud. CMORPH uses daily snow/ice maps generated by the NOAA/National Environmental Satellite, Data and Information Services for screening surface snow/ice (Joyce et al., 2007). This high precipitation value for winter might be the result of averaging all the pixels to get the catchment precipitation. As a result the fit between the two data sets is poor. R^2 of 0.54 is obtained between CMORPH and in-situ precipitation (Figure 25 A).

This is in agreement with Xie et al. (2007) who investigated the performance of CMORPH over East Asia and found that except for the north-western part of China, correlation was generally low in western China with close to zero correlation computed over northern Tibet. They also found that CMORPH precipitation product accuracy was good during warmer and wetter season than during colder seasons.

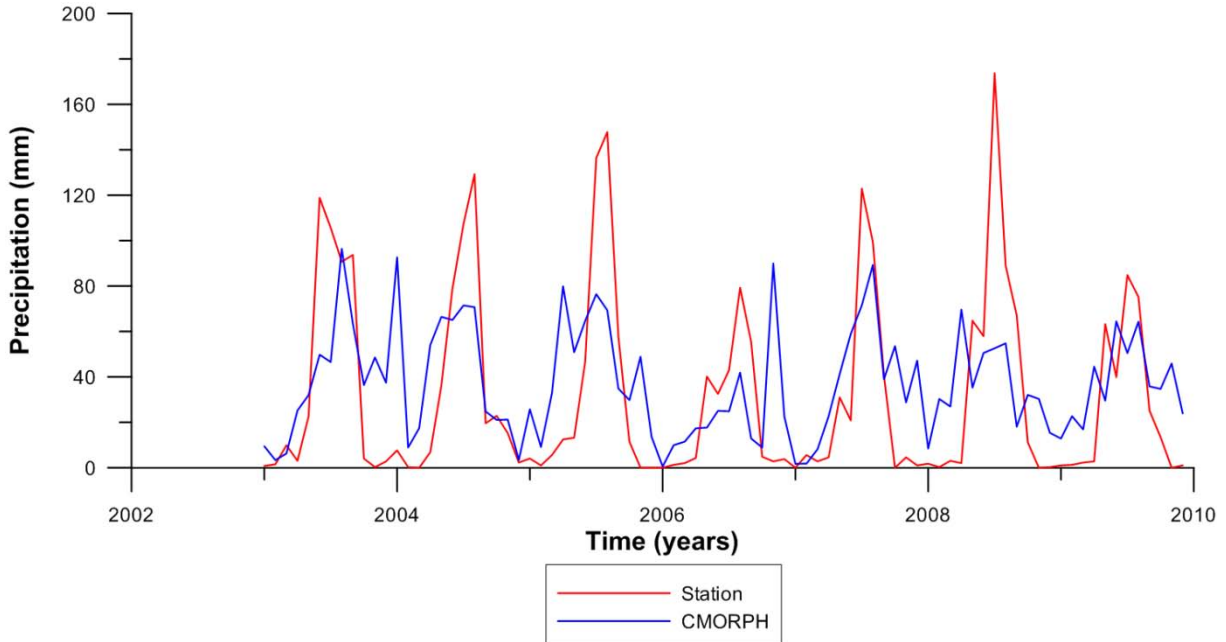


Figure 23. Monthly CMORPH and Bangoin station precipitation

On the other hand, GLDAS monthly precipitation has a good fit with measurements at Bangoin (Figure 25 B) with R^2 of 0.85. GLDAS is able to produce the monthly trend of precipitation recorded at Bangoin (Figure 24), with disagreement only in 2005 seasons where GLDAS is recording significantly low precipitation than in the station. These differences can be explained by the distance of station from the catchment (Figure 2). Precipitation varies spatially so some difference is inevitable, but the overall trend is well represented.

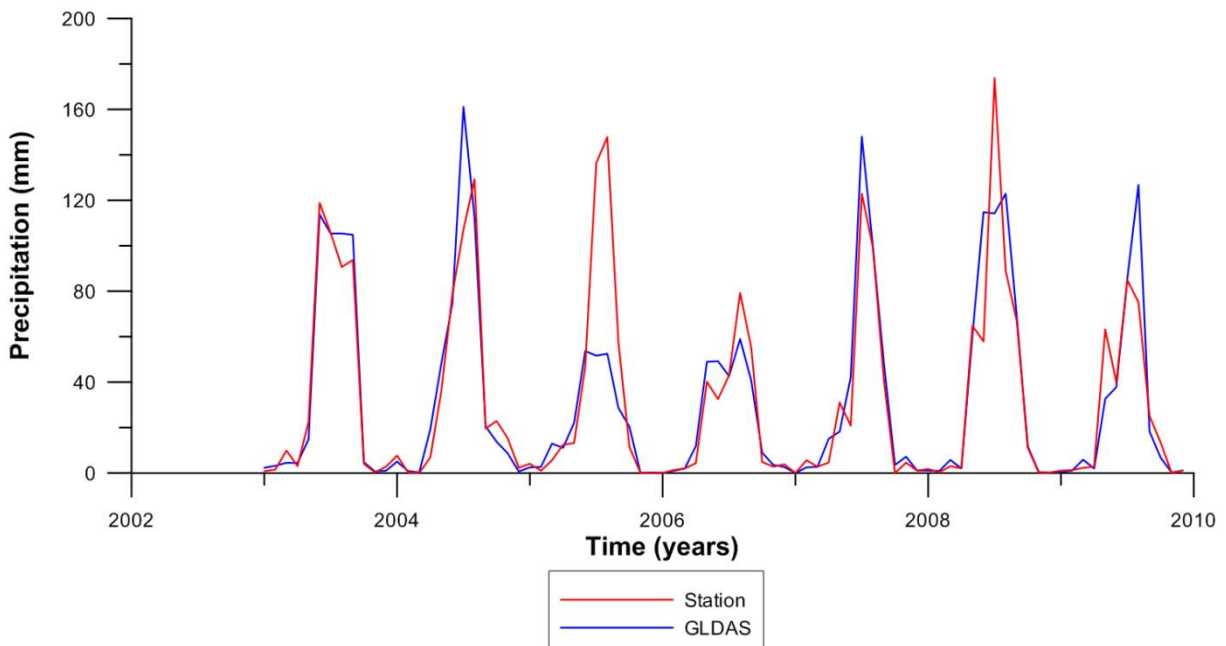


Figure 24. Monthly GLDAS and Bangoin station precipitation

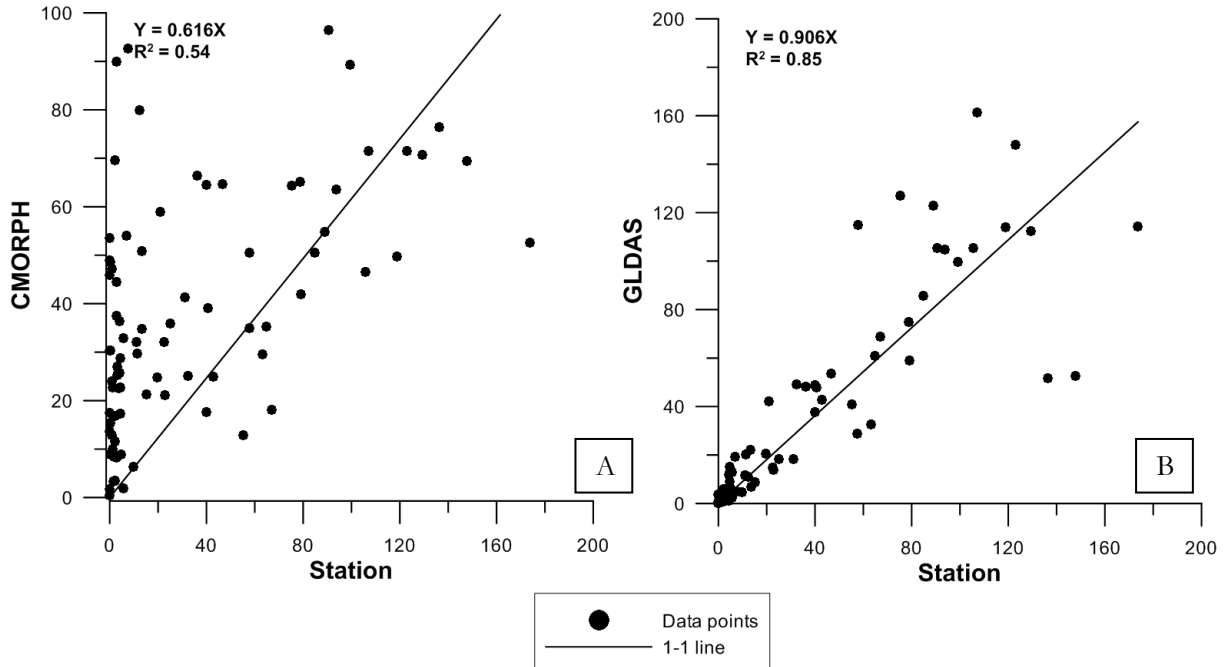


Figure 25. (A) CMORPH – Station correlation. (B) GLDAS – Station correlation

Annual GLDAS precipitation plot is shown in Figure 26. Annually precipitation did not change much. In 2008 highest annual precipitation was measured, which is associated with an early onset of Indian monsoon on the plateau (Kang et al., 2009).

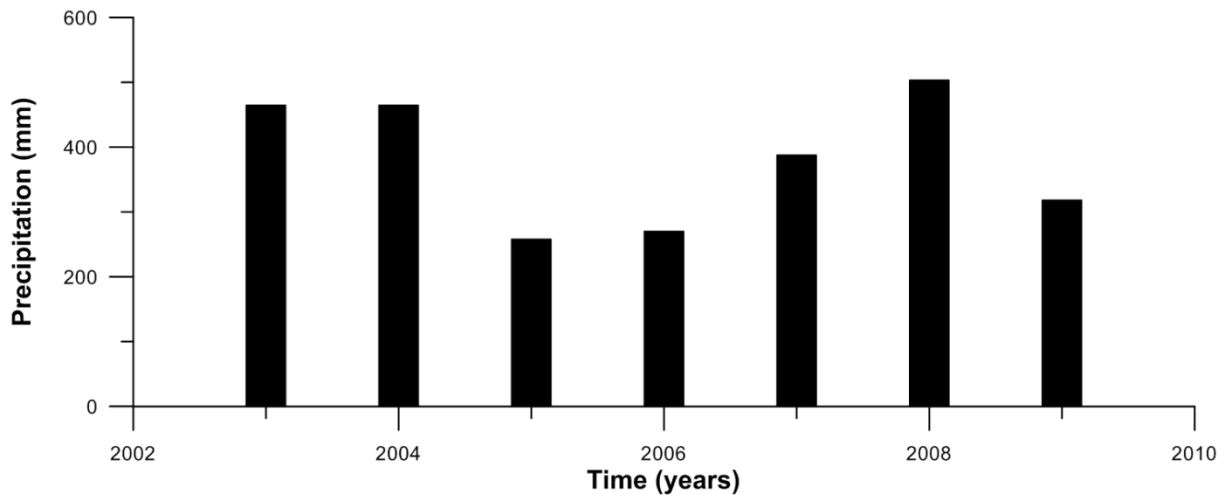


Figure 26. Annual sum of GLDAS rainfall on Namco catchment.

4.4. Evaporation

Annual sum of GLDAS evaporation plot is shown in Figure 27. This is evaporation for the land surface as LSM's do not simulate evaporation from open water. The figure shows that the simulated land evaporation does not show much change over the study period. In these estimates the lake evaporation is not taken into consideration. However, from experience we know that lake evaporation is typically larger than that of land.

Chen et al. (2006) and Zhang et al. (2007) investigated the evaporation trend over the whole Tibetan plateau and found it to be decreasing, under increasing air temperature. They found the decrease in evaporation was related to decrease in wind speed and sunshine duration. So, the use of evaporation estimates that rely on air temperature and radiation (e.g. Priestley-Taylor (Priestley & Taylor, 1972), Thornthwaite (Thornthwaite, 1948)) is not suitable for Tibetan Plateau. With rising trend of air temperature on Tibetan Plateau reported (Wu et al., 2007; Xu et al., 2008), the use of air temperature dependent evaporation method will lead to wrong estimation of evaporation. Chen et al. (2005) compared evaporation obtained with Thornthwaite method with those obtained from pan evaporation and Penman - Monteith equation. They found under increasing air temperature the trend by Thornthwaite method was also increasing which was not according to those as of pan and Penman - Monteith method.

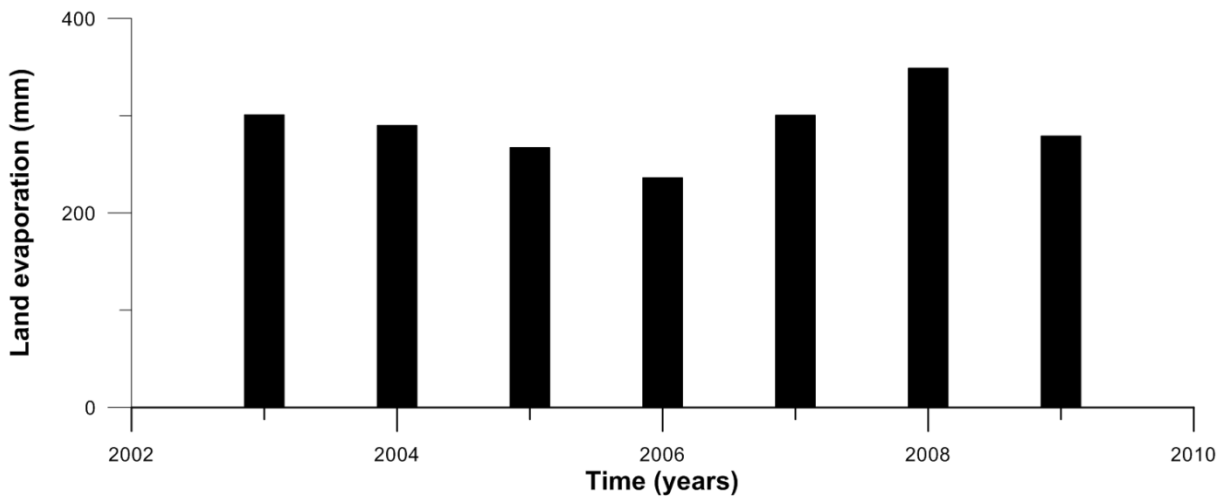


Figure 27. Annual sum of land evaporation from Namco catchment

Lake evaporation will be evaluated based on nearby big lakes (Selin Co and Yamdrok Yamtso) where pan evaporation measurements were available (Figure 28). Xu et al. (2009) investigated Yamdrok Yamtso lake for the time period of 1961 – 2005 and found that lake evaporation decreased by 7%, this trend was not found in land evaporation. Same decreasing evaporation trend was also observed for the time period of 1975 – 2008 for Selin Co Lake (Bian et al., 2010). Studies based on earlier time period (Krause et al., 2010; Liu et al., 2010; Zhu et al., 2010) than ours using pan evaporation data from Bangoin station also reported decreasing trend in evaporation from the Namco Lake. So based on these findings we may assume that also for our period the evaporation from Namco Lake is decreasing.

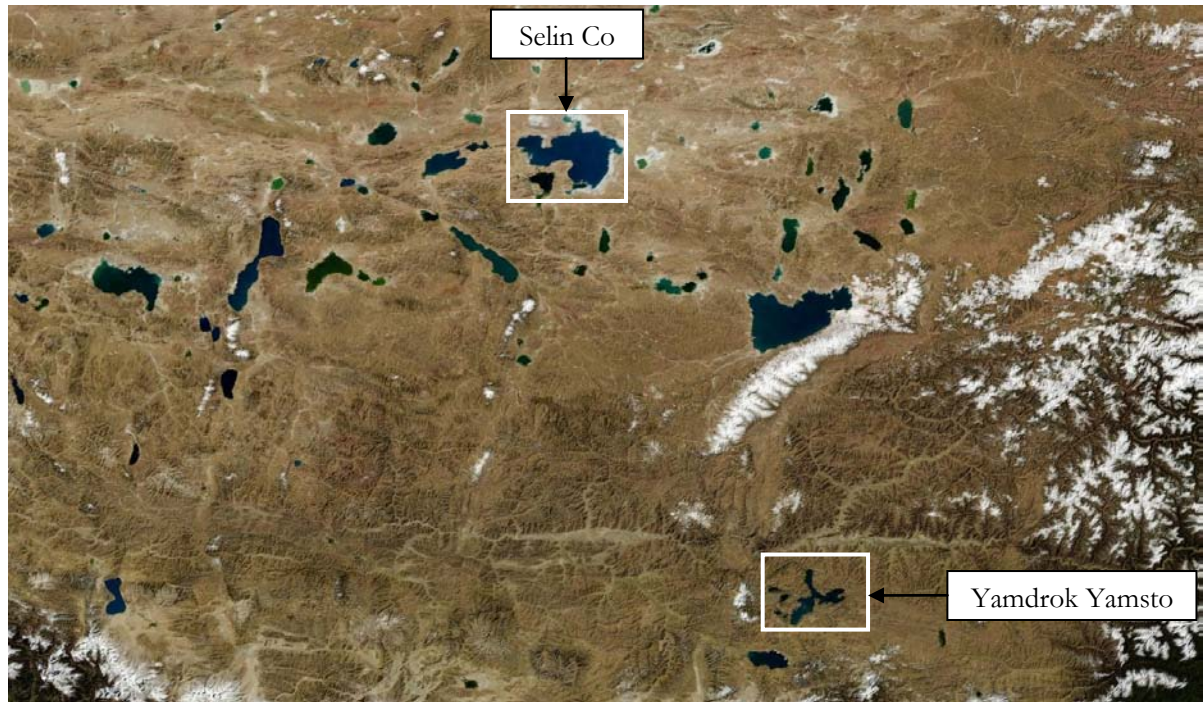


Figure 28. Location of Selin Co and Yamdrok Yamsto Lake

4.5. Runoff

As already mentioned in section 2, the main source of runoff feeding the lake is glaciers distributed in Nyainqentanghla Mountain range. As we do not have runoff measurement available an attempt will be made to relate the glacier melt with precipitation and temperature.

Two main factors which affect the glacier mass balance is air temperature and precipitation, the key factor being temperature (Singh & Kumar, 1997). Precipitation which falls in the form of snow helps maintain the glacier mass balance. Snow has high albedo and thus reflects most of the sunlight keeping the temperature low, suppressing glacier melt. Figure 29 shows the annual GLDAS snowfall and air temperature of Namco catchment. Decrease in annual snowfall from 2006 onwards is in accordance with increase of water level obtained from altimeters. Less snow over the years decreases the albedo of the region, which in turn facilitates the glacier melt and also permafrost degradation by increasing the temperature. This fact is true in our case, the years with high snowfall has low temperature and vice versa (Figure 29). In case of year 2008 a disagreement is noticed between air temperature and snowfall. In 2008 prolonged summer monsoon season was reported (Kang et al., 2009) which lowered the temperature. It is clear that from the onset of 2006, the lake level rise registered by the altimeter is because of the glacier melt runoff increase and permafrost degradation due to high temperature. High precipitation observed in 2008 helped to maintain the water level in the following years.

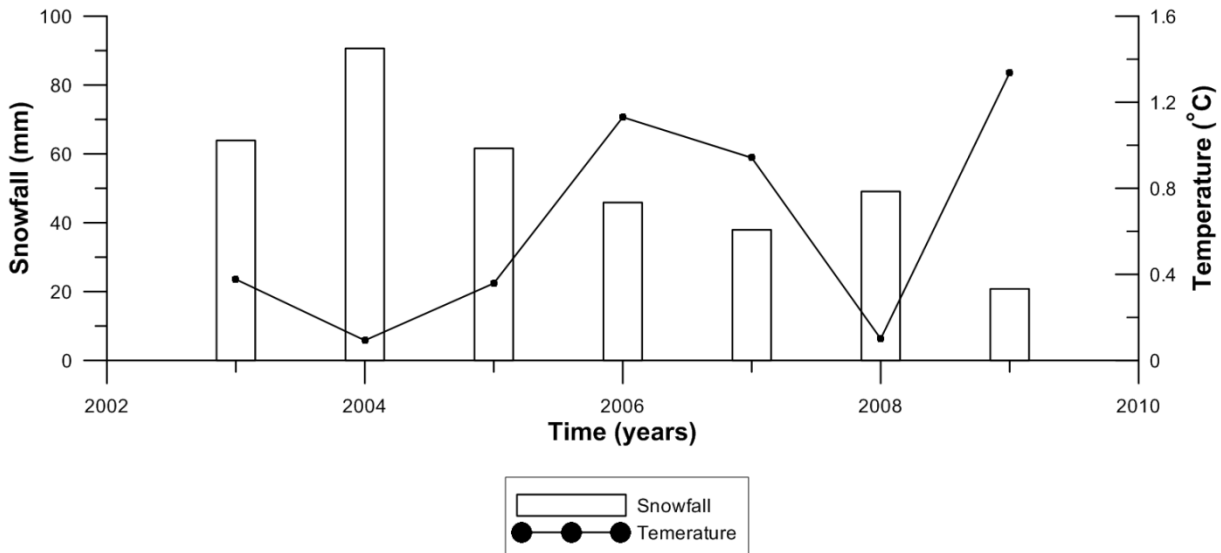


Figure 29. Annual sum of GLDAS snowfall and corresponding mean air temperature

Fujita et al. (2007) investigated Tanggula glacier in Tibetan Plateau and found melt to be sensitive to change in precipitation and temperature on seasonal basis, although these changes only slightly altered annual averages. In order to study the variations seasonally we divided the months with temperature $> 0^{\circ}\text{C}$ as warm season and $< 0^{\circ}\text{C}$ as cold season. Figure 30 shows the seasonal rainfall and mean temperature plot. From the temperature plot we can see rise in temperature for both warm and cold seasons. Increase of temperature in warm season helps accelerate the glacier melt process, while the increase in winter temperature prolongs the ablation period. Both warm and cold season temperature rise help accelerate the glacier melt process. In case of rainfall the general trend in both warm and cold season is decreasing. Generally rainfall in these high regions occurs in the form of snow during winter. Less snow will help increase the temperature of the region facilitating the glacier melt process. In the warm season we see rise in rainfall after 2006. Rainfall decreases the snow albedo by surface wetting, which also facilitates the melting process. The findings is also supported by Zhou et al. (2010), they studied the runoff from Zhadang glacier on Nyainqentanghla Mountain for years 2007-2008 and found that in 2008 the runoff decreased by 53.8 % as result of precipitation increase of 17.9 % in 2008 with majority of precipitation in the form of snow.

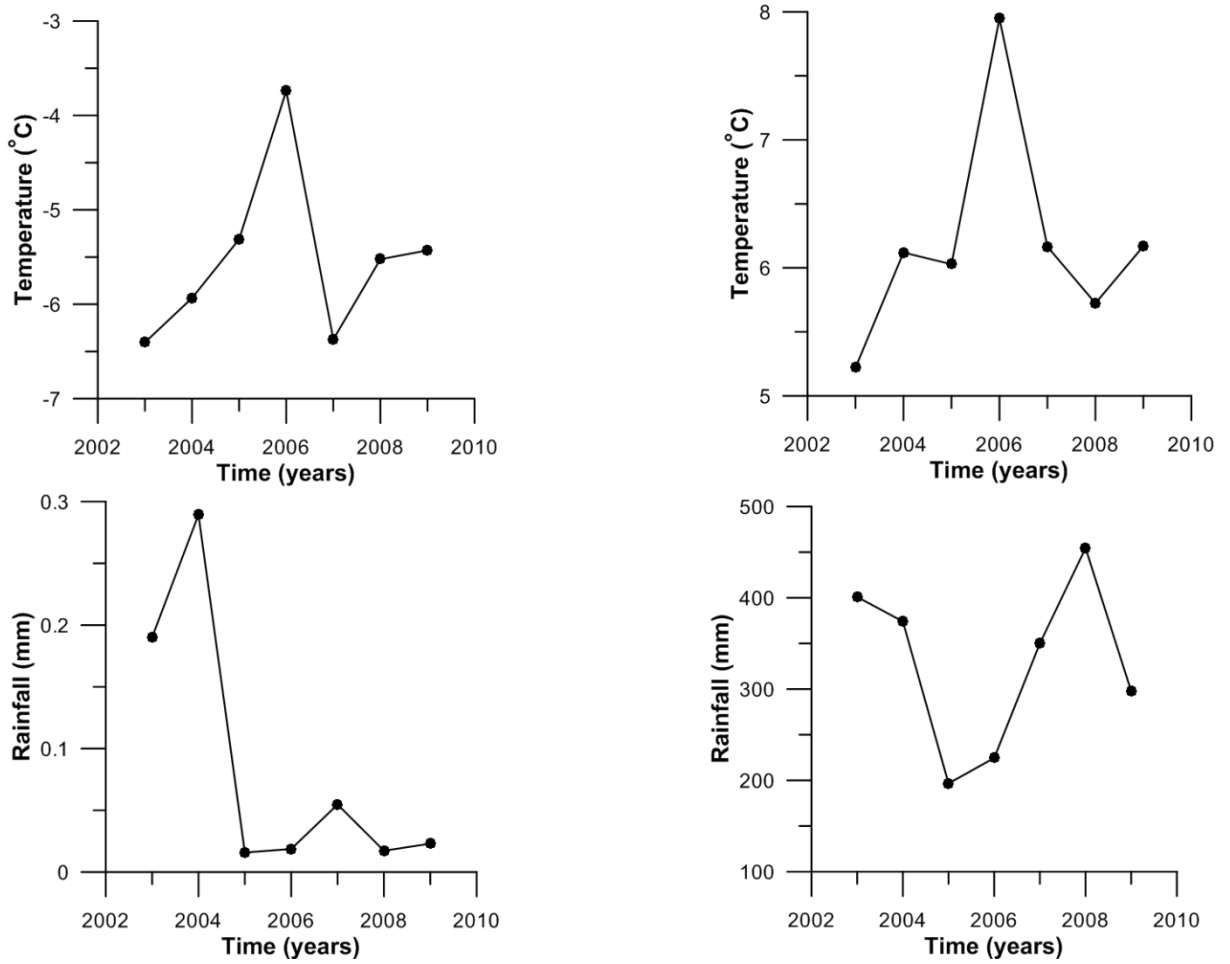


Figure 30. Seasonal variation of mean air temperature and GLDAS rainfall in cold season (left) and warm season (right) during 2003 – 2009.

5. CONCLUSIONS AND RECOMMENDATIONS

5.1. Conclusions

Studying the response of Namco Lake to change in atmospheric forcings of the Tibetan Plateau is the main objective of this study. Lake area was calculated by using grey level histogram thresholding technique based on ASAR WSM images. Lake level was obtained from space borne radar (ENVISAT RA-2) and laser (ICESat) altimetry. To evaluate the cause of changes in the lake area and level, we study the sources and sink (e.g. precipitation, evaporation and runoff) based on remote sensed and LSM products. The conclusions that can be drawn from this study are:

- During the study period of 2003 – 2009 the lake area has grown by 17 km² (0.86 %) and the lake level rose by more than 2 m. Both data sources demonstrate independently from each other that Namco Lake is growing.
- Space borne altimeters are able to measure the water level variations very well. Water level fluctuations obtained from both altimeters has an excellent fit with in-situ water level fluctuations, with R² of more than 0.86 and RMSD less than 0.15 m. Special attention needs to be given when using ENVISAT altimetry over the lake because of possibility of including land elevations in GDR's.
- GLDAS rainfall is able to represent catchment precipitation with R² of 0.84 when compared with near by station precipitation. Annually GLDAS precipitation did not change much. Studies conducted on Namco Lake in earlier time period than the presented results report on decreasing evaporation trends. Same decreasing evaporation trend was also reported by studies conducted on nearby Selin Co and Yamdrok Yamtso Lake. Mean annual air temperature over the study area increased with pronounced increase observed from 2006 onwards. As such, increase in lake area and level is because of increasing inflow into the lake from glacier melt and permafrost degradation as a result of increasing temperature during both warm and cold seasons. Decreasing evaporation also helps in lake growth process but in this thesis due to lack of data, actual evaporation from the lake could not be calculated. Water level rise accelerated from 2006 because of abrupt rise in temperature onwards, except for 2008 where high rainfall helped maintain the water level.

5.2. Recommendations

- Evaporation is one of the most important factors related to the lake water balance. So efforts must be made to quantify actual evaporation using data from Nam MI station and also investigate the pan evaporation measured.
- With the availability of runoff and precipitation data from the glaciers on Nyainqentanglha Mountains, a proper glacier mass balance should be carried out to quantify the glacier melt.
- Snow plays a vital role in maintaining the glacier mass balance, so an attempt needs to be made to collect the snow data on the Nyainqentanglha Mountain.

LIST OF REFERENCES

- Beniston, M., & Rebetez, M. (1996). Regional behavior of minimum temperatures in Switzerland for the period 1979–1993. *Theoretical and Applied Climatology*, 53(4), 231-243.
- Benveniste, J., Roca, M., Levrini, G., Vincent, P., Baker, S., Zanife, O., et al. (2001). The Radar Altimetry Mission: RA-2, MWR, DORIS and LRR. *ESA bulletin* - 106.
- Bian, D., Bian, B., La, B., Wang, C., & Chen, T. (2010). The Response of Water Level of Selin Co to Climate Change during 1975-2008. *Acta Geographica Sinica*, 65, 313-319.
- Bianduo, Bianbaciren, Li, L., Wang, W., & Zhaxiyangzong. (2009). The response of lake change to climate fluctuation in north Qinghai-Tibet Plateau in last 30 years. *Journal of Geographical Sciences*, 19(2), 131-142.
- Birkett, C. M. (1995). The contribution of TOPEX/POSEIDON to the global monitoring of climatically sensitive lakes. *J. Geophys. Res.*, 100(C12), 25179-25204.
- Chen, D., Gao, G., Xu, C.-Y., Guo, J., & Ren, G. (2005). Comparison of the Thornthwaite method and pan data with the standard Penman-Monteith estimates of reference evapotranspiration in China. *Climate Research*, 28(2), 123-132.
- Chen, S., Liu, Y., & Axel, T. (2006). Climate Change on the Tibetan plateau: Potential evapotranspiration trends from 1961 - 2000. *Climatic Change*, 76, 291-319.
- Crétaux, J.-F., & Birkett, C. (2006). Lake studies from satellite radar altimetry. *Comptes Rendus Geosciences*, 338(14-15), 1098-1112.
- ESA. (2000). Parameters affecting radar backscatter. from http://earth.esa.int/applications/data_util/SARDOCS/spaceborne/Radar_Courses/Radar_Course_II/parameters_affecting.htm
- ESA. (2007). ASAR Product Handbook
- ESA. (2009). ENVISAT RA-2/MWR Level 2 User Manual. 1.3.
- Frappart, F., Calmant, S., Cauhopé, M., Seyler, F., & Cazenave, A. (2006). Preliminary results of ENVISAT RA-2-derived water levels validation over the Amazon basin. *Remote Sensing of Environment*, 100(2), 252-264.
- Fujita, K., Ohta, T., & Ageta, Y. (2007). Characteristics and climatic sensitivities of runoff from a cold-type glacier on the Tibetan Plateau. *Hydrological Processes*, 21(21), 2882-2891.
- Joyce, R., Janowiak, J., Xie, P., & Arkin, P. (2007). CPC MORPHING Technique (CMORPH). In V. Levizzani, P. Bauer & F. J. Turk (Eds.), *Measuring Precipitation From Space* (Vol. 28, pp. 307-317): Springer Netherlands.
- Joyce, R. J., Janowiak, J. E., Arkin, P. A., & Xie, P. (2004). CMORPH: A Method that Produces Global Precipitation Estimates from Passive Microwave and Infrared Data at High Spatial and Temporal Resolution. *Journal of Hydrometeorology*, 5(3), 487-503.
- Kang, S., Chen, F., Zhang, Y., Yang, W., Yu, W., & Yao, T. (2009). Correspondance. Early onset of rainy season suppresses glacier melt: a case study on Zhadang glacier, Tibetan Plateau. *Journal of Glaciology*, 55(192), 755-759.
- Krause, P., Biskop, S., Helmschrot, J., Flugel, W.-A., Kang, S., & Gao, T. (2010). Hydrological system analysis and modelling of the Nam Co basin in Tibet. *Adv. Geosci.*, 27, 29-36.
- Kumar, S. V., Peters-Lidard, C. D., Tian, Y., Houser, P. R., Geiger, J., Olden, S., et al. (2006). Land information system: An interoperable framework for high resolution land surface modeling. *Environmental Modelling & Software*, 21(10), 1402-1415.
- Liu, J., Kang, S., Gong, T., & Lu, A. (2010). Growth of a high-elevation large inland lake, associated with climate change and permafrost degradation in Tibet. *Hydrology and Earth System Sciences*, 14(3), 481-489.
- Liu, J., Wang, S., Yu, S., Yang, D., & Zhang, L. (2009a). Climate warming and growth of high-elevation inland lakes on the Tibetan Plateau. *Global and Planetary Change*, 67(3-4), 209-217.
- Liu, X., & Chen, B. (2000). Climatic warming in the Tibetan Plateau during recent decades. *International Journal of Climatology*, 20(14), 1729-1742.
- Liu, X., Cheng, Z., Yan, L., & Yin, Z. (2009b). Elevation dependency of recent and future minimum surface air temperature trends in the Tibetan Plateau and its surroundings. *Global and Planetary Change*, 68(3), 164-174.

- Liu, X., & Zhang, M. (1998). Contemporary climatic change over the qinghai-xizang plateau and its response to the green-house effect. *Chinese Geographical Science*, 8(4), 289-298.
- Medina, C. E., Gomez-Enri, J., Alonso, J. J., & Villares, P. (2008). Water level fluctuations derived from ENVISAT Radar Altimeter (RA-2) and in-situ measurements in a subtropical waterbody: Lake Izabal (Guatemala). *Remote Sensing of Environment*, 112(9), 3604-3617.
- Mercier, F., Cazenave, A., & Maheu, C. (2002). Interannual lake level fluctuations (1993-1999) in Africa from Topex/Poseidon: connections with ocean-atmosphere interactions over the Indian Ocean. *Global and Planetary Change*, 32(2-3), 141-163.
- NASA. (2002). ICESAT Brochure.
- NSIDC. ICESat/GLAS FAQ. from <http://nsidc.org/data/icesat/faq.html>
- NSIDC. (2009). GLAS Altimetry Product Usage Guidance. 129.
- Oberstadler, R., Honsch, H., & Huth, D. (1997). Assessment of the mapping capabilities of ERS-1 SAR data for flood mapping: a case study in Germany. *Hydrological Processes*, 11(10), 1415-1425.
- Priestley, C. H. B., & Taylor, R. J. (1972). On the Assessment of Surface Heat Flux and Evaporation Using Large-Scale Parameters. *Monthly Weather Review*, 100(2), 81-92.
- Quartly, G. D., Srokosz, M. A., & Guymer, T. H. (1998). Understanding the effects of rain on radar altimeter waveforms. *Advances in Space Research*, 22(11), 1567-1570.
- Reis, S., & Yilmaz, H. M. (2008). Temporal monitoring of water level changes in Seyfe Lake using remote sensing. *Hydrological Processes*, 22(22), 4448-4454.
- Shuman, C. A., Zwally, H. J., Schutz, B. E., Brenner, A. C., DiMarzio, J. P., Suchdeo, V. P., et al. (2006). ICESat Antarctic elevation data: Preliminary precision and accuracy assessment. *Geophys. Res. Lett.*, 33(7), L07501.
- Singh, P., & Kumar, N. (1997). Impact assessment of climate change on the hydrological response of a snow and glacier melt runoff dominated Himalayan river. *Journal of Hydrology*, 193(1-4), 316-350.
- Telmer, K., & Costa, M. (2007). SAR-based estimates of the size distribution of lakes in Brazil and Canada: a tool for investigating carbon in lakes. *Aquatic Conservation: Marine and Freshwater Ecosystems*, 17(3), 289-304.
- Thorntwaite, C. W. (1948). An Approach Toward a Rational Classification of Climate. *Soil Science*, 66(1), 77.
- Wald, L. (1990). Monitoring the decrease of lake Chad from space. *Geocarto International*, 5(3), 31 - 36.
- Wu, S., Yin, Y., Zheng, D., & Yang, Q. (2007). Climatic trends over the Tibetan Plateau during 1971–2000. *Journal of Geographical Sciences*, 17(2), 141-151.
- Xie, P., Chen, M., Yang, S., Yatagai, A., Hayasaka, T., Fukushima, Y., et al. (2007). A Gauge-Based Analysis of Daily Precipitation over East Asia. *Journal of Hydrometeorology*, 8(3), 607-626.
- Xu, J., Yu, S., Liu, J., Haginoya, S., Ishigooka, Y., Kuwagata, T., et al. (2009). The Implication of Heat and Water Balance Changes in a Lake Basin on the Tibetan Plateau. *Hydrological Research Letters*, 3, 1-5.
- Xu, Z. X., Gong, T. L., & Li, J. Y. (2008). Decadal trend of climate in the Tibetan Plateau—regional temperature and precipitation. *Hydrological Processes*, 22(16), 3056-3065.
- Zhang, Y., Liu, C., Tang, Y., & Yang, Y. (2007). Trends in pan evaporation and reference and actual evapotranspiration across the Tibetan Plateau. *J. Geophys. Res.*, 112(D12), D12110.
- Zheng, D., & Li, B. (1999). Progress in studies on geographical environments of the Qinghai-Xiang plateau. *Chinese Geographical Science*, 9(4), 289-296.
- Zhou, S., Kang, S., Gao, T., & Zhang, G. (2010). Response of Zhadang Glacier runoff in Nam Co Basin, Tibet, to changes in air temperature and precipitation form. *Chinese Science Bulletin*, 55(20), 2103-2110.
- Zhou, X., Zhao, P., Chen, J., Chen, L., & Li, W. (2009). Impacts of thermodynamic processes over the Tibetan Plateau on the Northern Hemispheric climate. *Science in China Series D: Earth Sciences*, 52(11), 1679-1693.
- Zhu, L., Xie, M., & Wu, Y. (2010). Quantitative analysis of lake area variations and the influence factors from 1971 to 2004 in the Nam Co basin of the Tibetan Plateau. *Chinese Science Bulletin*, 55(13), 1294-1303.
- Zink, M., Torres, R., Buck, C. H., Rosich, B., & Closa, J. (2002). Calibration and early results of the ASAR on ENVISAT. *IEEE International Geoscience and Remote Sensing Symposium (IGARSS'02)*, 596-598.
- Zwally, H. J., Schutz, R., Bentley, C., Bufton, J., Herring, T., Minster, J., et al. (2003). GLAS/ICESat L2 Global Land Surface Altimetry Data. 18.

APPENDICES

APPENDIX A: Acquisition date of ERS-1 and ERS-2 images

S.N.	Date	Satellite
1	6/18/1992	ERS-1
2	7/4/1992	ERS-1
3	8/27/1992	ERS-1
4	10/1/1992	ERS-1
5	10/17/1992	ERS-1
6	11/5/1992	ERS-1
7	11/21/1992	ERS-1
8	12/10/1992	ERS-1
9	1/30/1993	ERS-1
10	2/18/1993	ERS-1
11	3/6/1993	ERS-1
12	3/25/1993	ERS-1
13	4/10/1993	ERS-1
14	4/29/1993	ERS-1
15	9/16/1993	ERS-1
16	10/2/1993	ERS-1
17	7/25/1994	ERS-1
18	8/14/1994	ERS-1
19	10/14/1995	ERS-1
20	10/30/1995	ERS-1
21	1/8/1996	ERS-1
22	4/7/1996	ERS-2
23	4/22/1996	ERS-1
24	4/23/1996	ERS-2
25	5/11/1996	ERS-2
26	5/12/1996	ERS-2
27	5/28/1996	ERS-2
28	8/25/1996	ERS-2
29	9/29/1996	ERS-2
30	10/15/1996	ERS-2
31	4/8/1997	ERS-2
32	6/1/1997	ERS-2
33	6/17/1997	ERS-2
34	11/4/1997	ERS-2
35	12/9/1997	ERS-2
36	1/13/1998	ERS-2
37	2/17/1998	ERS-2
38	3/24/1998	ERS-2
39	4/28/1998	ERS-2
40	6/2/1998	ERS-2

41	7/26/1998	ERS-2
42	9/17/1998	ERS-2
43	4/13/1999	ERS-2
44	11/9/1999	ERS-2
45	12/14/1999	ERS-2
46	10/24/2000	ERS-2
47	6/10/2001	ERS-2
48	6/26/2001	ERS-2
49	7/31/2001	ERS-2
50	8/19/2001	ERS-2
51	12/18/2001	ERS-2
52	1/6/2002	ERS-2
53	1/22/2002	ERS-2
54	4/21/2002	ERS-2
55	7/20/2003	ERS-2
56	7/4/2004	ERS-2
57	7/22/2004	ERS-2
58	8/8/2004	ERS-2
59	1/11/2005	ERS-2
60	2/8/2009	ERS-2
61	2/24/2009	ERS-2
62	3/31/2009	ERS-2

APPENDIX B: Acquisition date of ASAR IM images.

S.N.	Date
1	4/6/2003
2	4/22/2003
3	5/11/2003
4	6/15/2003
5	7/20/2003
6	8/5/2003
7	9/28/2003
8	11/2/2003
9	11/18/2003
10	12/7/2003
11	12/23/2003
12	1/11/2004
13	1/27/2004
14	2/15/2004
15	3/21/2004
16	5/30/2004
17	6/15/2004
18	7/20/2004
19	8/13/2004
20	9/11/2004
21	11/2/2004
22	11/21/2004
23	12/7/2004
24	12/26/2004
25	7/24/2005
26	8/28/2005
27	9/2/2005
28	12/11/2005
29	1/15/2006
30	2/8/2006
31	4/30/2006
32	6/4/2006
33	7/9/2006
34	8/13/2006
35	10/22/2006
36	11/15/2006
37	11/26/2006
38	12/20/2006
39	2/20/2007
40	3/11/2007
41	4/15/2007

42	5/1/2007
43	5/20/2007
44	6/5/2007
45	6/24/2007
46	7/10/2007
47	7/29/2007
48	8/14/2007
49	9/2/2007
50	9/18/2007
51	10/7/2007
52	10/23/2007
53	11/11/2007
54	11/27/2007
55	4/23/2008
56	5/4/2008
57	5/9/2008
58	7/13/2008
59	9/21/2008
60	10/26/2008
61	12/16/2008
62	1/4/2009
63	1/20/2009
64	2/24/2009
65	3/14/2009
66	3/15/2009
67	3/31/2009
68	4/19/2009
69	5/5/2009
70	5/24/2009
71	5/29/2009
72	6/9/2009
73	6/28/2009
74	8/2/2009
75	8/26/2009
76	9/6/2009
77	9/22/2009
78	10/16/2009
79	10/27/2009
80	11/15/2009
81	12/9/2009
82	12/20/2009
83	1/24/2010
84	2/9/2010
85	2/28/2010

86	3/16/2010
87	4/4/2010
88	5/9/2010
89	5/25/2010
90	6/2/2010
91	6/13/2010
92	6/29/2010
93	7/18/2010
94	8/3/2010

APPENDIX C: ASAR WSM image date and lake area

Image Date	Area (km²)
8/2/2003	1971
7/25/2004	1991
8/25/2005	1998
8/6/2006	1984
8/19/2007	1991
8/22/2008	2000
8/15/2009	1988

APPENDIX D: ENVISAT RA-2 water level

Date	Water Level (m)
10/19/2002	4725.70
11/23/2002	4725.69
12/28/2002	4725.39
2/1/2003	4725.16
3/8/2003	4724.95
4/12/2003	4725.45
5/17/2003	4725.35
6/21/2003	4725.22
7/26/2003	4725.89
10/4/2003	4726.30
11/8/2003	4726.53
6/5/2004	4726.01
8/14/2004	4726.67
3/17/2007	4726.48
4/21/2007	4726.92
5/26/2007	4726.67
8/4/2007	4726.77
9/8/2007	4727.08
10/13/2007	4733.48
11/17/2007	4733.14
12/22/2007	4732.54
3/1/2008	4726.49
4/5/2008	4726.50
5/10/2008	4726.39
6/14/2008	4726.52
7/19/2008	4726.95
8/23/2008	4727.19
9/27/2008	4727.40
11/1/2008	4727.35
12/6/2008	4727.19
1/10/2009	4727.23
2/14/2009	4726.86
3/21/2009	4726.62
4/25/2009	4727.26
5/30/2009	4727.00
7/4/2009	4727.03
8/8/2009	4727.25
9/12/2009	4727.35
10/17/2009	4727.28
11/27/2009	4727.07

APPENDIX E: ICESat water level

Date	Water Level (m)
2/23/2003	4723.67
3/3/2003	4723.46
3/11/2003	4724.27
3/19/2003	4724.18
3/27/2003	4724.28
9/27/2003	4725.42
11/7/2003	4725.01
10/25/2003	4724.90
2/25/2004	4724.85
3/10/2004	4724.83
5/26/2004	4724.68
6/9/2004	4724.92
10/12/2004	4725.70
10/26/2004	4725.51
11/6/2004	4725.70
2/27/2005	4724.86
3/12/2005	4725.11
3/24/2005	4726.01
5/29/2005	4725.04
6/11/2005	4725.39
10/30/2005	4726.01
11/12/2005	4725.94
3/2/2006	4725.45
3/27/2006	4724.95
6/1/2006	4725.65
6/15/2006	4725.85
11/2/2006	4725.73
11/16/2006	4725.73
11/27/2006	4725.75
3/20/2007	4725.45
4/2/2007	4725.55
4/14/2007	4725.62
10/11/2007	4725.85
10/24/2007	4725.79
2/25/2008	4725.41
3/10/2008	4725.45
3/21/2008	4725.51
10/12/2008	4726.23
12/6/2008	4726.15
12/17/2008	4726.18
3/17/2009	4725.86

10/9/2009	4726.12
-----------	---------